Hindawi
Journal of Nanomaterials
Volume 2022, Article ID 2446972, 27 pages
https://doi.org/10.1155/2022/2446972

Research Article

Analysis of Forced Convection with Hybrid Cu-Al_2O_3 Nanofluids Injected in a Three-Dimensional Rectangular Channel Containing Three Perpendicular Rotating Blocks with $\kappa - \varepsilon$ Turbulent Modeling

S. H. Elhag,[1] Abid A. Memon,[2] M. Asif Memon,[2,3] Kaleemullah Bhatti,[2] Kavikumar Jacob,[3] Samirah Alzahrani,[1] and Jamel Seidu[4]

[1]*Department of Mathematics and Statistics, College of Science, Taif University, P.O. Box 11099, Taif 21944, Saudi Arabia*
[2]*Department of Mathematics and Social Sciences, Sukkur IBA University, Sukkur, 65200 Sindh, Pakistan*
[3]*Department of Mathematics and Statistics, Faculty of Applied Sciences and Technology, Universiti Tun Hussein Onn Malaysia, Batu Pahat, 86400 Johor, Malaysia*
[4]*School of Railways and Infrastructure Development, University of Mines and Technology (UMaT) Essikado, Sekondi-Takoradi, Ghana*

Correspondence should be addressed to Jamel Seidu; jseidu@umat.edu.gh

Received 18 May 2022; Revised 18 June 2022; Accepted 28 June 2022; Published 19 July 2022

Academic Editor: Zafar Said

In this paper, the flow of hybrid nanofluids in a three-dimensional rectangular channel consisting of three perpendicular blocks will be analyzed in terms of heat transfer. The two perpendicular rectangular blocks are rotating with speed ω. The hybrid mixture consists of aluminum oxide and copper, and each of them will contain in volume fraction of 0.001 to 0.25. The κ-ε model of turbulent flow along with Navier and energy equation will be brought into action by using the finite element package COMSOL Multiphysics 5.6. Volume fraction and speed of rotation will be used as the parameters, and a parameter study will be done by fixing the Reynolds number Re = 50,000 with energy dissipation rate (ε) (m^2/s^3) ($3.46E-6$ to $3.76E-5$), kinetic energy (κ) (m^2/s^2) ($2.50E-06$ to $1.23E-05$), and the Prandtl number (0.98506 to 1.2625). It was deducted that the local Nusselt number is minimized at the outlet for stationary blocks and the maximum for the moving blocks. In addition, the mean number of Nusselt on the upper surface of the rectangular channel increases when the blocks are stationary and decreases when the blocks are moving. The study suggests that to maximize the conduction process in the channel the blocks must rotate with a certain velocity. This study also determined that with increasing the total viscosity of hybrid nanofluids, the average temperature is decreasing linearly in the middle of the channel whether the blocks are rotating or not. The temperature gradient along the z-axis decreases with increasing volume fraction only when blocks are stationary. In addition, it has been determined that the maximum average temperature occurs when the volume fractions of copper and oxide are equal to 0.001.

1. Introduction and Literature Survey

The study of imposing a hybrid nanofluid in the domain to increase the heat transfer rate is increasing these days due to having a large number of applications in industrial development. The hybrid nanofluid can be a mixture of metallic, nonmetallic, and polymeric nanosized particles which are suspended in pure fluid like water and ethanol glycol. It was approved by many researchers with and without experiment, adding nanofluid in the pure fluid will increase the heat transfer rate. At Argonne National Laboratory, the first experiment based on nanofluid was performed [1]. In this experiment for the first time, the tremendous properties of the nanofluid in terms of heat transfer were explained. In

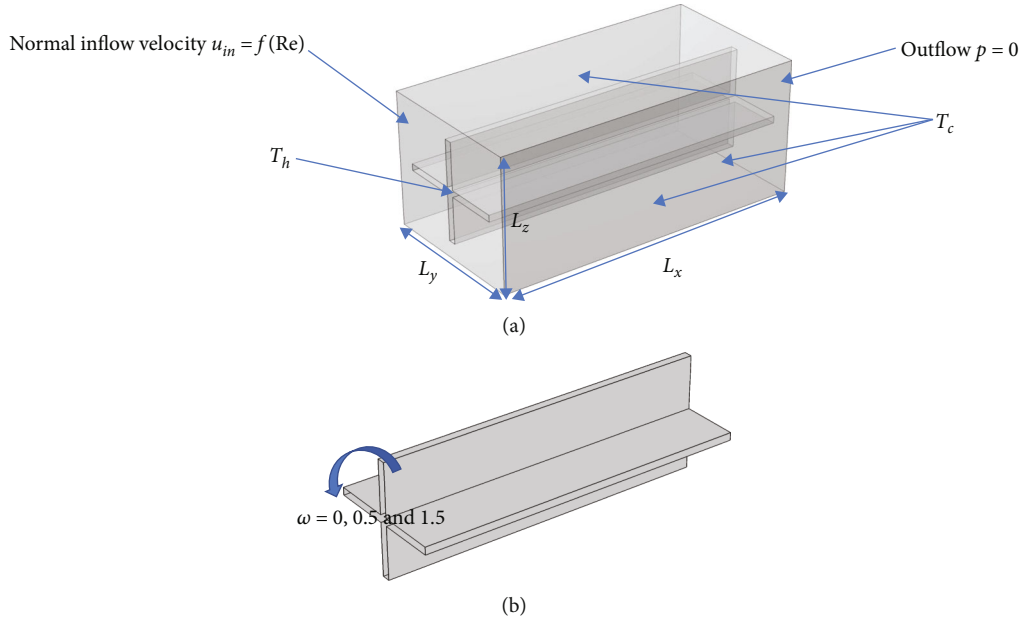

Figure 1: (a, b) Schematic diagram of the three-dimensional rectangular channel containing the perpendicular blocks.

the experiment, it was also suggested to improve these properties by certain modifications. The study beings a revolution in the field of engineering due to having a large number of applications of heat production. Later, several experimental and numerical investigations for heat transfer have been done by taking nanofluids under consideration [2, 3]. The applications of the nanofluids can also be seen in making efficient heat exchanger tubes. In the research study [4], WO_3/water-based nanofluids were investigated in the triple tube for the purpose to produce an efficient heat exchanger. The tube was comprised of a porous plate along with the rib type and twisted tape. In [5], a survey was written about the advantage of nanofluids when used as the coolant to make the efficient heat exchangers. In the survey, the author reported several findings regarding the previous literature which contribute to increasing the rate of heat transfer, like pressure drop, Reynolds number, flow regime, temperature, kind of base fluid, and the size of nanomaterials. Later on, the recent advancements in the thermophysical properties of the nanofluid were discussed in [6] along with the heat transport, dynamic motion, and the new challenges while studying the heat transportation with the help of nanofluids. The author of this article specially discussed the heat transport and the dynamic motion of the nanofluids in the media. The applications of nanofluids can largely be seen in making efficient solar collectors. For example, in [7], the hybrid nanofluids were used to observe the heat transfer by using the two nanofluids copper and aluminum oxide in the solar collector. It was found that the copper nanofluids have a finer capability than the aluminum oxide to hike up the heat transfer up to 6.4%. In producing efficient batteries, the flow of nanofluid along the heat transfer was also investigated in [8]. In this article, the author used the most advanced technique of machine learning on the experimental data of viscosity and density of the ternary nanofluids at various temperatures to improve the performance of the battery. Recently, the study of mixing the different nanofluids is gaining importance due to their reliable results for heat production in the interested domain. The concept of hybrid nanofluid was initiated [9, 10] with experiments and numerical solutions. It was suggested by them that the usage of hybrid nanofluid will increase more heat transfer rate as compared to an individual nanofluid through the base fluid. After that idea, several researchers started working on better understanding the hybrid nanofluids. A copper tube was investigated for the Al_2O_3-water nanofluid flow through several experiments [11–14]. With these experiments, it was explained that including the Al_2O_3 nanoparticles will boost the convection process in the copper tube, and also, it is much enhanced by increasing the Reynolds number and the concentration of the nanoparticles. The impact on the heat transfer by the constant magnetic effect as well as radiation on the stretching sheets was investigated in [15] while taking the water as the base fluid with copper and aluminum oxide as nanofluids. It was found that the constant magnetic effect and the radiation both enhance the rate of heat transfer. From many experiments [16–20], it is proved that even mixing a small amount of any nanoparticles or copper with the aluminum oxide will improve the thermal conductivity without harming the strongness of the nanofluids. The tremendous mixture of Cu-Al_2O_3 which is mostly used to analyze the convection process in the channel is formed by implementing the hydrogen reduction reaction on the CuO-Al_2O_3 combination [21]. It can also be produced by blending the pure Al_2O_3 and the very small-sized nanoparticles of CuO [22–24]. Also, the mixture CuO-Al_2O_3 has various importance in the engineering field. Among them, one of the applications is used there for the heat distribution in the electronic heat sink production [25–27]. The application of this mixture can widely be found in making efficient solar collectors [28, 29].

Table 1: Thermophysical properties of the nanofluid and parameters to geometry building [30].

Symbol	Value	Explanation
ϕ_1	0.001, 0.01, 0.09, 0.1, and 0.25	Volume fraction of aluminum oxide
ϕ_2	0.001, 0.01, 0.09, 0.1, and 0.25	Volume fraction of copper
ρ_{np1}	3880 (kg/m^3)	Density of alumina
ρ_{np2}	8954 (kg/m^3)	Density of copper
ρ_{np}	$\left(\phi_1\rho_{np1} + \phi_2\rho_{np2}\right)/\phi_1 + \phi_2$	The total density of the nanoparticles
$(c_p)_{np1}$	765 (J/kgK)	Specific heat of aluminum oxide
$(c_p)_{np2}$	383.1 (J/kgK)	Specific heat of copper
$(c_p)_{np}$	$\phi_1\rho_{np1}(c_p)_{np1} + \phi_2\rho_{np2}(c_p)_{np2}/\varphi\rho_{np}$	Specific heat of particles
ϕ	$\phi_1 + \phi_2$	The total volume fraction of nanoparticles
κ_{np1}	40 (W/mK)	Thermal conductivity of the aluminum oxide
κ_{np2}	386 (W/mK)	Thermal conductivity of copper
κ_{np}	$\phi_1\kappa_{np1} + \phi_2\kappa_{np2}/\phi_1 + \phi_2$	Total thermal conductivity of nanofluids
ρ_{bf}	998 (kg/m^3)	The density of the base fluid
ρ_{nf}	$\rho_{bf}(1-\phi) + \phi\rho_{np}$	Density of nanofluid
$(c_p)_{bf}$	4182 (J/kgK)	Specific heat of the base fluid
$(c_p)_{nf}$	$\rho_{bf}(1-\phi)(c_p)_{bf} + \rho_{np}(1-\phi)(c_p)_{np}/\rho_{nf}$	Specific heat capacity of nanofluid
κ_{bf}	0.597 (W/mK)	Thermal conductivity of the base fluid
κ_{nf}	$\kappa_{bf}\left(\kappa_{np} + 2\kappa_{bf} + 2\left(\kappa_{np} - \kappa_{bf}\right)\phi/\kappa_{np} + 2\kappa_{bf} - \left(\kappa_{np} - \kappa_{bf}\right)\phi\right)$	Thermal conductivity of the nanofluids
μ_{bf}	0.000998 (Pa s)	The viscosity of the base fluid
μ_{hnf}	$\mu_{bf}/(1-\phi)^{2.5}$ (Pa s)	Viscosity of nanofluid
D_h	0.333 (cm)	Hydraulic diameter
Re	50,000	Reynolds number
u_{in}	μ_{hnf} Re$/\rho_{nf}D_h$	Inlet velocity
L_x	1 (cm)	Length along the x-axis
L_y	0.5 (cm)	Length along the y-axis
L_z	0.5 (cm)	Length along the z-axis
ω	0, 0.5, and 1.5 (m/s)	The rotational velocity of perpendicular blocks along the z-direction
T_c	293.15 (K)	Cold temp
T_h	323.15 (K)	Hot temp

The object of this study is to observe the heat distribution by passing a hybrid mixture of Cu-Al_2O_3 through the three-dimensional rectangular channel which contained the perpendicular blocks of a certain thickness. The perpendicular blocks are rotated with some speed. The problem is simulated by using the latest and emerging finite element package COMSOL Multiphysics 5.6 by using the Navier-Stokes equation, energy equation, and $\kappa - \varepsilon$ model of turbulent flow. By considering different volume fractions of the contents of the mixture with some speed of the perpendicular blocks, the parametric study for the heat transfer of the mixture contents will be observed. In the first section, we will describe the problem formulation along with the thermophysical properties of the chosen nanofluid. In the 2nd section, we will apply the mesh independent study and compare the results for the average Nusselt number with the available correlations from the literature. In the 3rd section, we will calculate the results for average temperature, temperature gradient, local Nusselt number, and average Nusselt number on the chosen domain. And, finally, we will write the conclusion. The selected geometry has not been discussed in the previous research work.

2. Problem Formulation

In the current research article, we are going to establish a simulation for the heat transfer and a turbulent flow in the three-dimensional rectangular channel containing the two

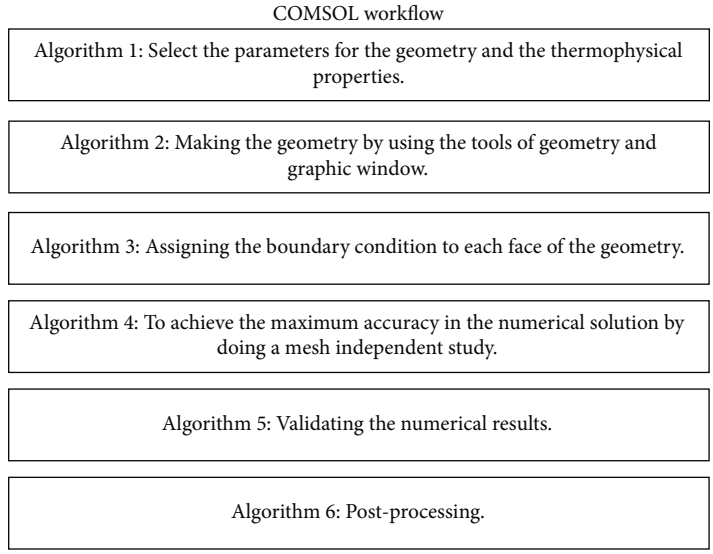

Figure 2: Working wagon wheel of COMSOL Multiphysics 5.6.

perpendicular rectangular blocks with a certain thickness. A hybrid-type nanofluid containing the aluminum oxide and copper in the water base fluid will be undergone from the inlet of the channel. The perpendicular blocks inside the three-dimensional channel are capable to rotate along the z -axis at the speed of ω. Let $L_x \times L_y \times L_z$ be the dimensions of the three-dimensional rectangular channel, and then, the thickness of perpendicular blocks will be taken as 5% of the length of the channel L_x and the gap ratio from the side of the channel is taken to $12.5\%L_y$; see Figures 1(a) and 1(b). A zero-pressure value is taken at the outlet of the channel and an average velocity u_{in} profile which is the function of the Reynolds number will be imposed from the left entrance of the channel. The perpendicular block will be allowed to rotate along the z-axis at a uniform speed ω. Let the surrounding of the channel bear a cool temperature T_c and the perpendicular blocks are facing a hot temperature T_h. A hybrid nanofluid composed of aluminum oxide and copper mixed with the water is under observation. Let subscript (1) present the aluminum oxide and subscript (2) present the thermophysical properties of copper, and then, we are in a position to explain all parameters to develop this simulation in Table 1.

The present model of hybrid nanofluid will be investigated by using the finite element package of COMSOL Multiphysics 5.6 in the space coordinate system. The three-dimensional incompressible Navier-Stokes is along with $\kappa - \varepsilon$ turbulence model of Reynolds Navier-Stokes equations. Let the velocity field of the flow be presented by the vector $\mathbf{u} = <u, \text{v}, \text{w}>$, and then, the governing partial differential equations and the energy equations are given as follows:

Continuity equation:

$$\rho_{\text{nf}}(\nabla \cdot \mathbf{u}) = 0. \tag{1}$$

Momentum equation:

$$\rho_{\text{nf}}(\mathbf{u} \cdot \nabla)\mathbf{u} = \nabla \cdot \left[-pI + (\mu_{\text{hnf}} + \mu_T)(\nabla \mathbf{u} + (\nabla \mathbf{u})^T\right]. \tag{2}$$

$\kappa - \varepsilon$ turbulence model:

$$\begin{aligned}
\rho_{\text{nf}}(\mathbf{u} \cdot \nabla)\kappa &= \nabla \cdot \left[\left(\mu_{\text{hnf}} + \frac{\mu_T}{\sigma_\kappa}\right)\nabla\kappa\right] + p_\kappa - \rho_{\text{nf}}\varepsilon, \\
\rho_{\text{nf}}(\mathbf{u} \cdot \nabla)\varepsilon &= \nabla \cdot \left[\left(\mu_{\text{hnf}} + \frac{\mu_T}{\sigma_\kappa}\right)\nabla\varepsilon\right] + c_{\varepsilon 1}\frac{\varepsilon}{\kappa} - c_{\varepsilon 2}\rho_{\text{nf}}\frac{\varepsilon^2}{\kappa},
\end{aligned} \tag{3}$$

where

$$\begin{aligned}
\mu_T &= \rho_{nf} c_\mu \frac{\kappa^2}{\varepsilon}, \\
p_\kappa &= \mu_T\left[\nabla \mathbf{u} : (\nabla \mathbf{u} + (\nabla \mathbf{u})^T\right], \\
&\rho_{\text{nf}}\left(c_p\right)_{\text{nf}}\mathbf{u} \cdot \nabla T = 0.
\end{aligned} \tag{4}$$

Boundary conditions:

Inlet: $x = 0, 0 \le y \le L_y, 0 \le z \le L_z$: $U_{\text{av}} = u_{\text{in}}$, $\kappa_0 = (3/2)(U_{\text{in}} I_T)^2$, $\varepsilon_0 = c_\mu^{3/2}(\kappa_0{}^{3/2}/L_T)$, $\partial T/\partial n = 0$.

Outlet: $x = \text{L}_x, 0 \le z \le L_z, 0 \le y \le L_y : p = 0, \nabla\kappa \cdot \mathbf{n} = 0$ and $\nabla\varepsilon \cdot \mathbf{n} = 0, \partial T/\partial n = 0$.

Along the outer surface of the rectangular box: a no-slip condition $u = 0, v = 0, w = 0$ will be imposed with $T = T_c$ and $\nabla\kappa \cdot \mathbf{n} = 0, \varepsilon = \rho_{\text{nf}}(c_\mu \kappa^2/\kappa_v \delta_w^+ \mu_{\text{nf}})$.

Along with the blocks $u = 0$, $v = 0$, and $w = \omega$, $\nabla\kappa \cdot \mathbf{n} = 0$ and $\nabla\varepsilon \cdot \mathbf{n} = 0$ and $\text{T} = \text{T}_c$, where n is the normal vector to the surface of the selected boundary $I_T = 0.05$, $L_T = 0.01850$, and $\delta_w^+ = 11.06$.

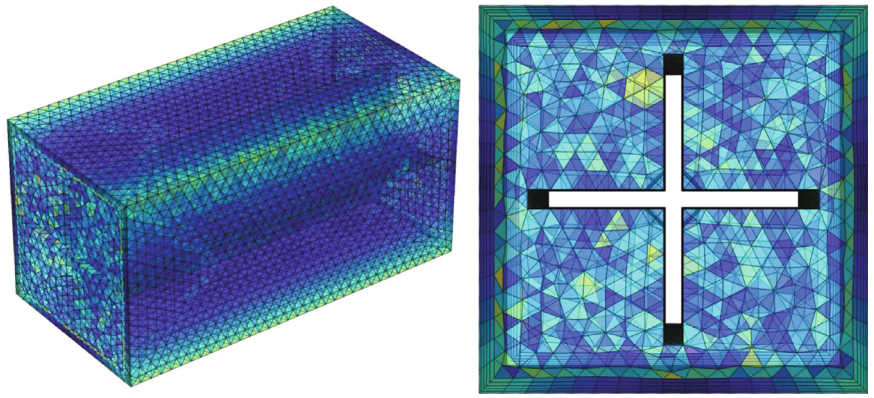

Figure 3: Schematic diagram of the meshing procedure in the twisted rectangular channel with tetrahedral elements.

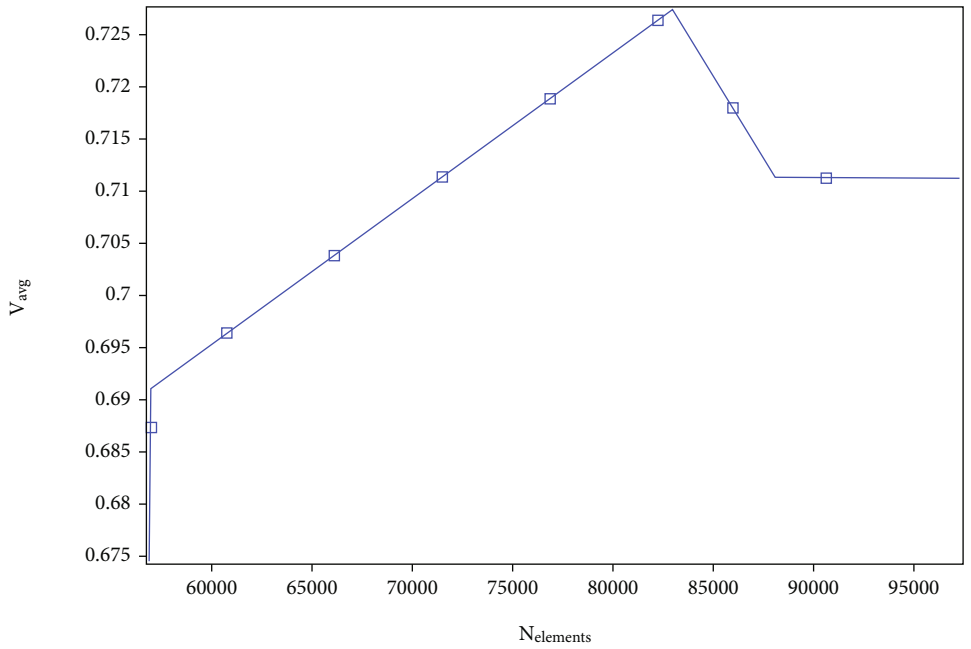

Figure 4: Average velocity magnitude at the outlet of twisted tube channel at Re = 50,000 and $\phi = \phi_1 + \phi_2 = 0.002$.

Turbulence variable:

$C_{\varepsilon 1}$	$C_{\varepsilon 2}$	C_μ	σ_κ	σ_ε	κ_v
1.44	1.92	0.09	1	1.3	0.41

2.1. Computational Parameters. Finally, we are enlisting the computational parameters as follows:

(i) Prandtl number: $\mathrm{Pr} = \mu_{\mathrm{hnf}}(c_p)_{\mathrm{nf}}/\kappa_{\mathrm{nf}}$

(ii) Heat flux: $Q = (\kappa_{\mathrm{nf}}/\kappa_f)\nabla T$

(iii) Heat transfer coefficient: $h = Q/A(T - T_b)$

(iv) Bulk temperature: $T_b = \int_\Omega \mathbf{u}T\, d\Omega / \int_\Omega \mathbf{u}\, d\Omega$

(v) Local Nusselt number: $\mathrm{Nu} = h\,x/k_{\mathrm{nf}}$

(vi) Average Nusselt number: $\mathrm{Nu}_{\mathrm{avg}} = (1/A)\int_\Omega \mathrm{Nu}_x\, dA$ where A is the area of the selected boundary

The governing equations given above subject to the boundary conditions will be considered to obtain the numerical solution by using the COMSOL Multiphysics 5.6 software. The software implements the finite element procedure to discretize the governing partial differential equation into a set of algebraic equations, and then, the set of algebraic equations will be solved by the Newton-Raphson procedure. About 75 simulations will be obtained by using the parametric study for the volume fraction of aluminum oxide and copper along with the rotational speed of the perpendicular blocks. The working algorithms of COMSOL software are given above; see Figure 2.

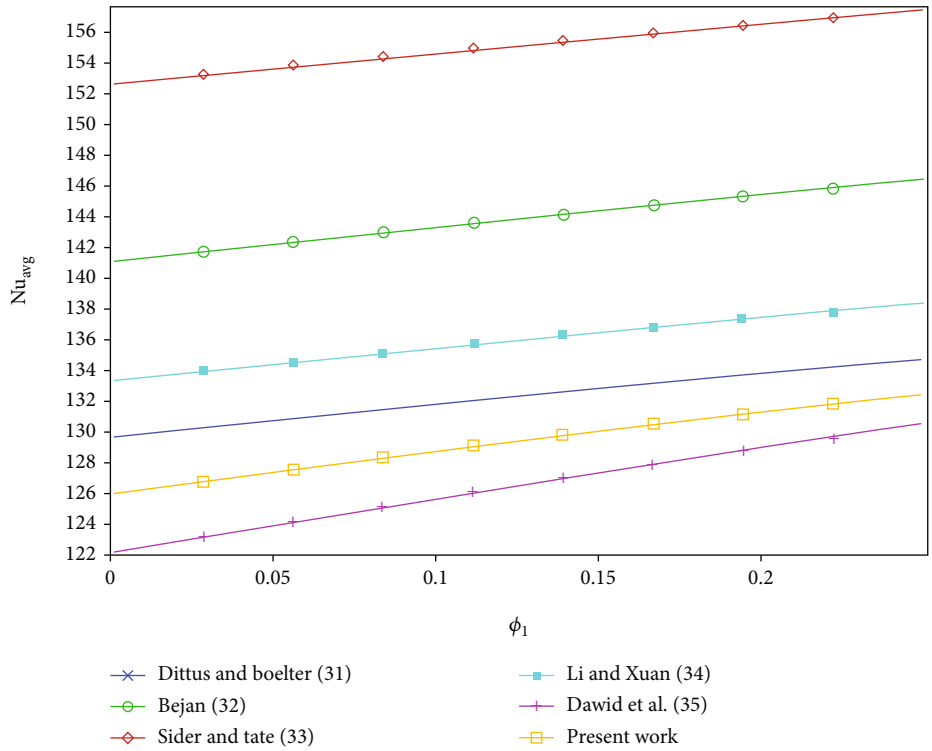

Figure 5: Validation and comparison of average Nusselt number at the exit of the channel against ϕ_1 when Re = 50,000, $\phi_2 = 0.001$, and $\omega = 0$.

Table 2: Average Nusselt number at the outlet of the channel against volume fraction of Al_2O_3.

ϕ_1	[31]	[32]	[33]	[34]	[35]	Present work
0.001	129.6963	141.0264	152.6951	133.3071	122.1352	125.9100
0.01	129.8972	141.245	152.891	133.5125	122.4697	126.1830
0.09	131.6322	143.1327	154.5806	135.2858	125.3763	128.5140
0.1	131.8412	143.3602	154.784	135.4996	125.7287	128.987
0.25	134.612	146.3746	157.4765	138.3343	130.4428	132.5200

3. Mesh Independent Study

To get the maximum accuracy level for a numerical method that is based on the meshing process, the mesh independent procedure will be the crucial step. According to the procedure, a targeted variable will be chosen at a certain boundary or location in the interested domain and then finding the numerical solution by increasing the number of elements. A point is reached where the numerical solution for the targeted variable will not be improved further. It is the stage where the numerical results will have reliable accuracy. For the current problem, the meshing process is applied to the selected three-dimensional geometry by using the various types of elements, i.e., tetrahedral, prisms, triangles, and quads; see Figure 3. The number of elements used is between 55,000 and 100,000; see Figure 4. The average velocity was chosen at the exit of the channel. The numerical results were obtained by using Re = 50,000, $\phi = 0.002$, and $\omega = 0$ where the volume fraction of aluminum oxide and copper is equal by the value of 0.001. It can be seen that as the number of elements is increased, the numerical solution for the average velocity at the outlet of the channel is improved. The solution gets the mesh independent stage when the number of elements is greater than 88,000.

Table 3: The percentage errors with Dittus-Boelter and Dawid et al.

ϕ_1	[31]	[35]
0.001	2.919359	3.09067
0.01	2.859338	3.03202
0.09	2.368873	2.50263
0.1	2.164877	2.59153
0.25	1.554096	1.59242

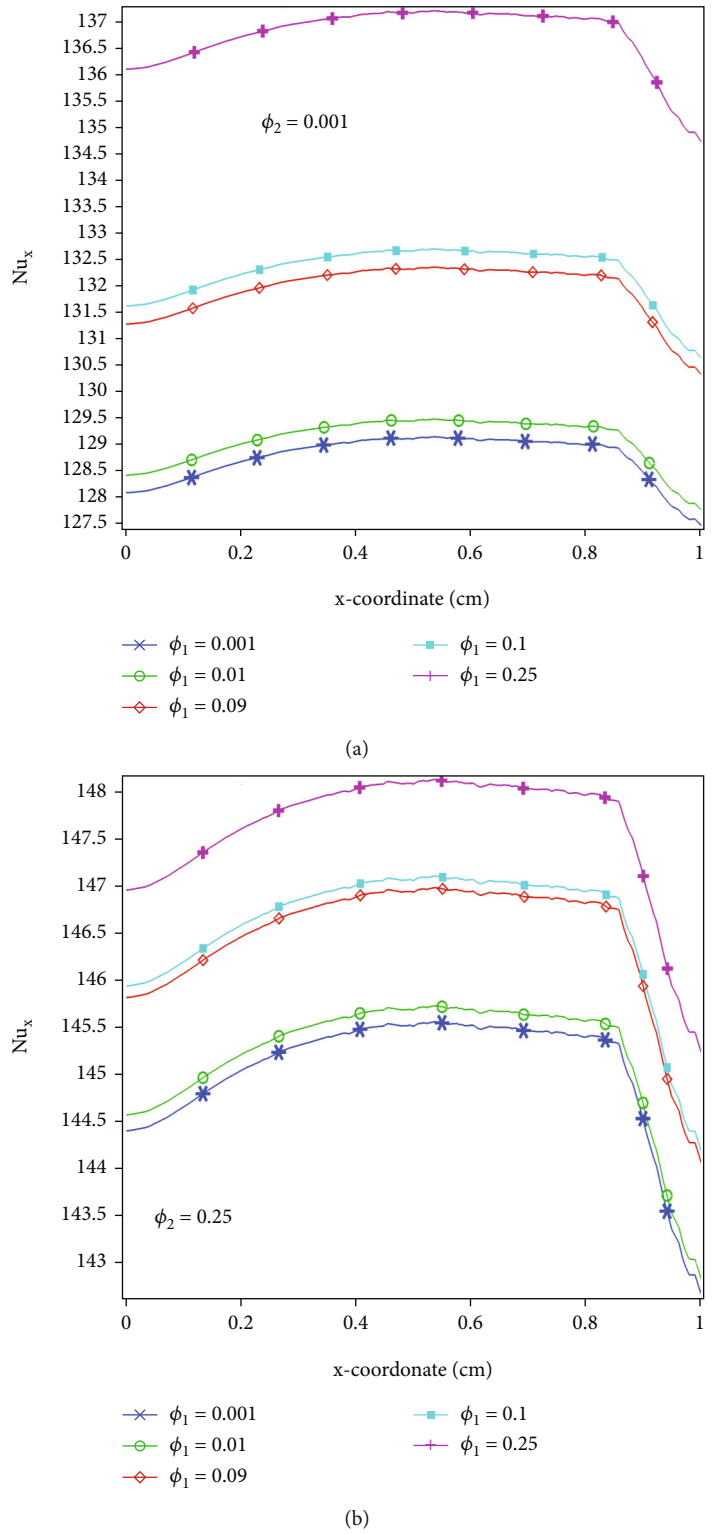

FIGURE 6: (a, b) Local Nusselt number along the length of the channel for all volume fractions of aluminum oxide at $\omega = 0$.

4. Validation and Comparison with Various Correlations

After doing the mesh independent study, the numerical solution obtained with FEM will be compared with the correlations of the average Nusselt number given in the literature [31–35]. Five different correlations are compared with the present work of the average Nusselt number at the outlet of the channel; see Figure 5. It can be seen in Table 2 that the present work for the average Nusselt number nearly satisfies

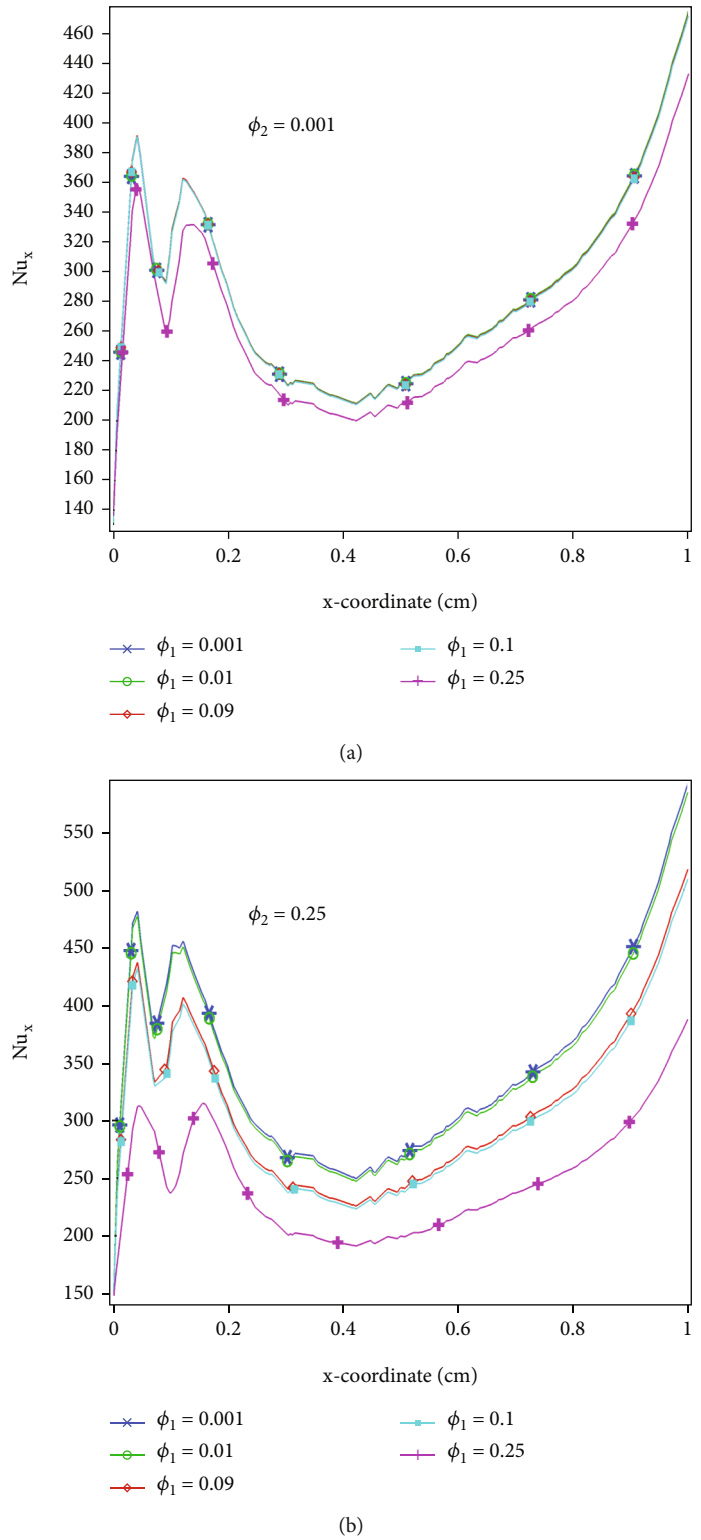

Figure 7: (a, b) Local Nusselt number along the length of the channel for all volume fractions of aluminum oxide at $\omega = 0.5$.

the experimental result of the Dittus-Boelter equation [31] and the numerical result of Dawid et al. [35] for the average Nusselt number.

Moreover, it can be perceived from Table 3 that, as we increase the volume fraction of aluminum oxide in the mixture, the percentage error is decreasing.

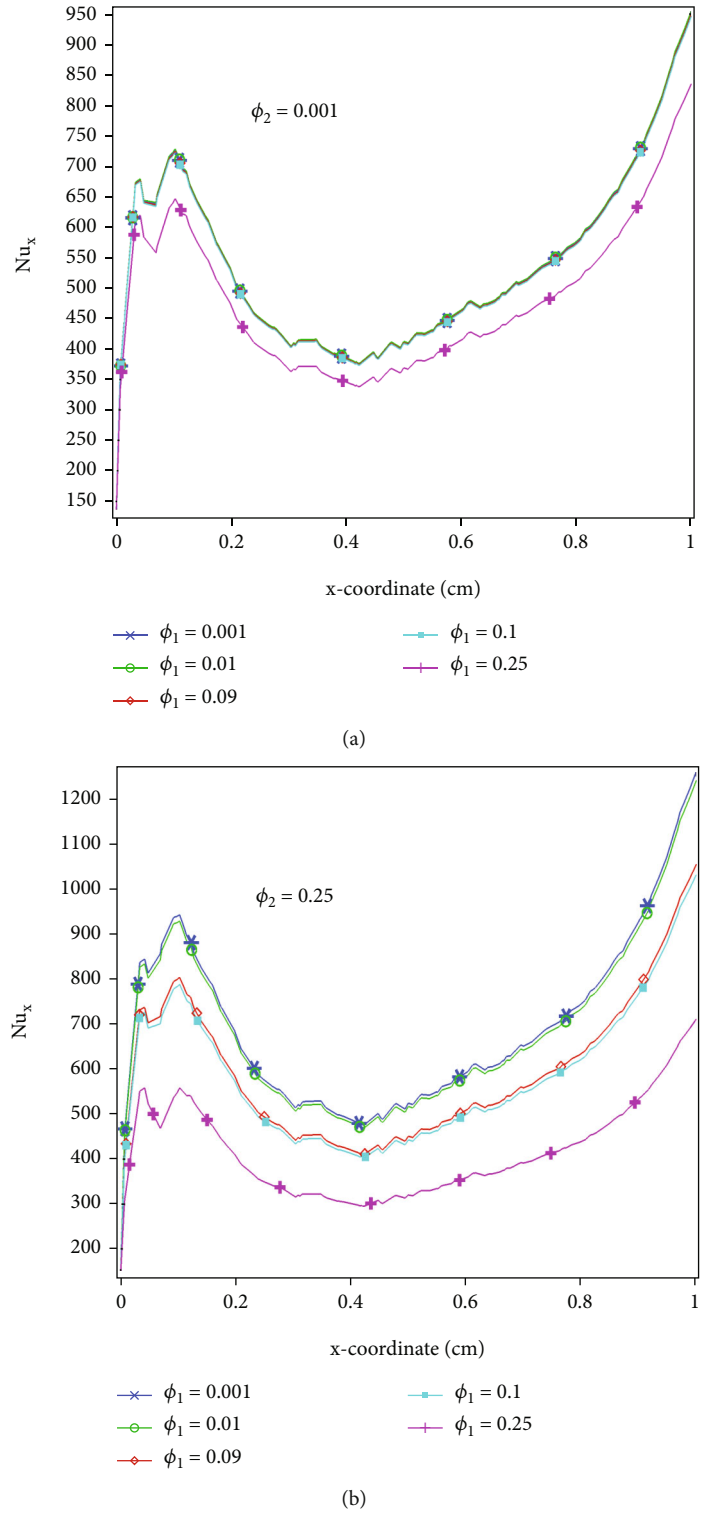

Figure 8: (a, b) Local Nusselt number along the length of the channel for all volume fractions of aluminum oxide at $\omega = 1.5$.

5. Result Discussion

5.1. Local and Average Nusselt Number. In this section, we are going to discuss the impact of the volume fraction of aluminum oxide and the copper on the local and average Nusselt number along the x-direction of the channel and altering the speed of the perpendicular blocks. The schema to check the pattern is like that of any two of the three parameters ϕ_1, ϕ_2, and ω and will be fixed and one will be changed.

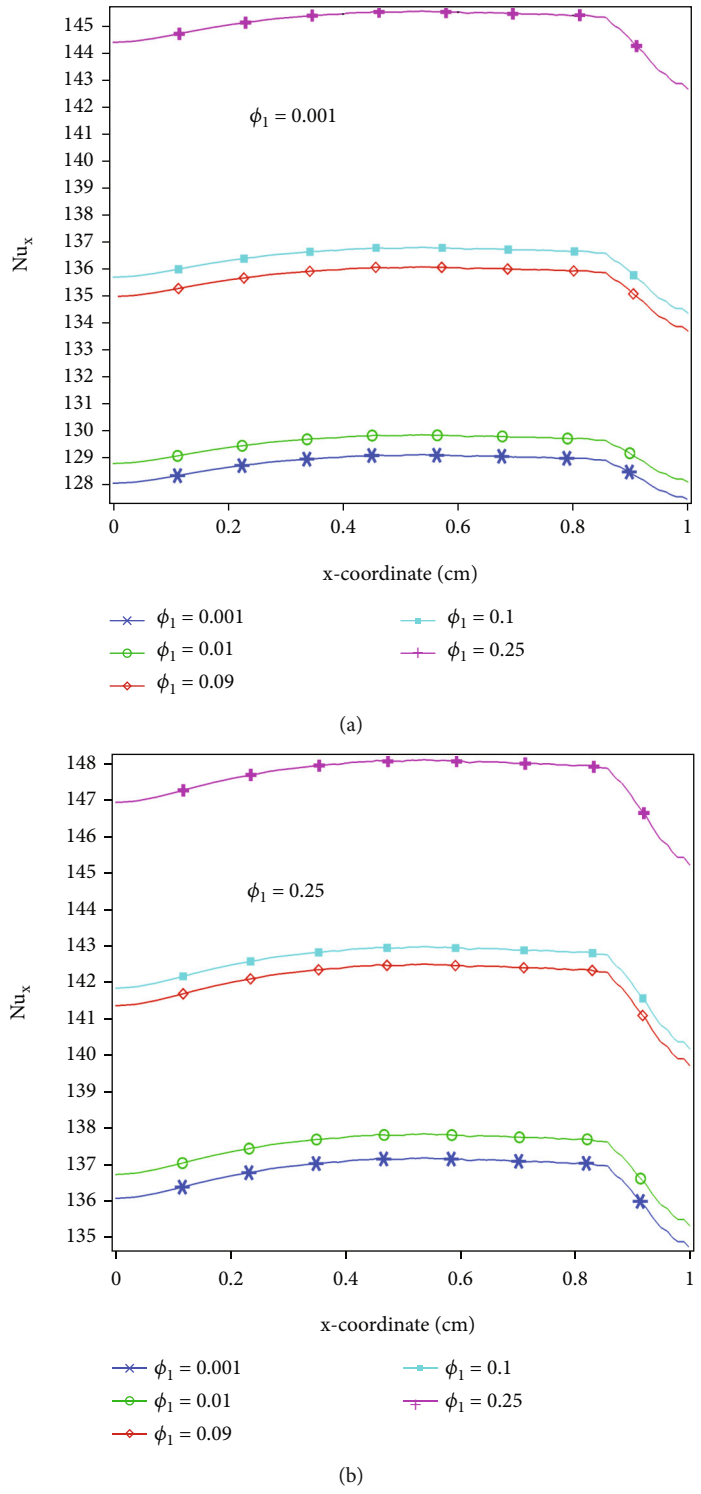

Figure 9: (a, b) Local Nusselt number along the length of the channel for all volume fractions of copper at $\omega = 0$.

Figures 6(a) and 6(b) are produced by fixing the volume fraction of the copper (0.001 and 0.25) and the speed of the perpendicular block ($\omega = 0$), and then, the impact of the local Nusselt number is checked by increasing the volume fraction of aluminum oxide. In Figure 6(a), it can be seen that the local Nusselt number is increasing along the x-direction first and then declined near the outlet of the channel when $\phi_2 = 0.001$, although, with the increasing volume fraction for aluminum oxide (0.001-0.25), the local Nusselt number is improved gradually along the x-direction of the channel. Figure 6(b) is produced by fixing $\phi_2 = 0.25$ and $w = 0$; it can be seen that the local Nusselt number along

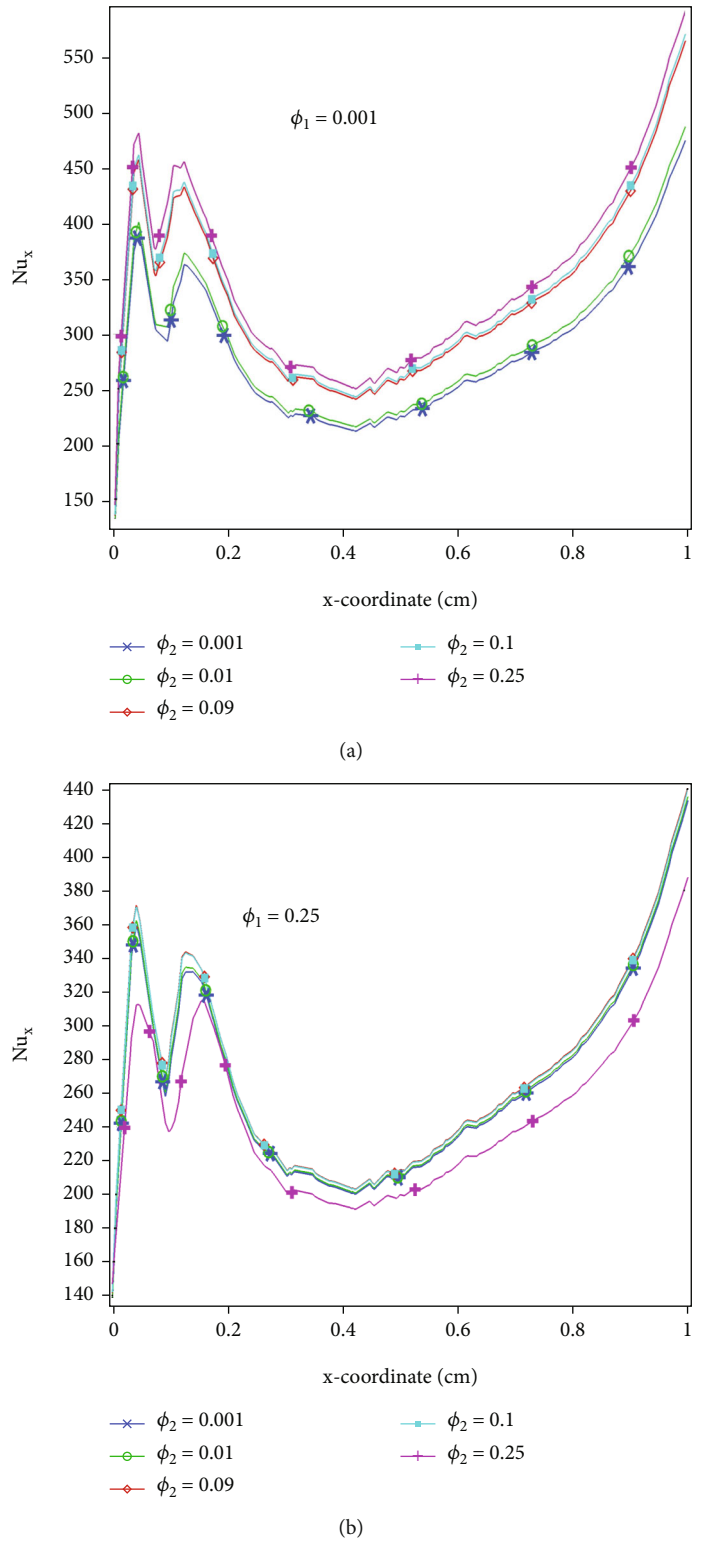

FIGURE 10: (a, b) Local Nusselt number along the length of the channel for all volume fractions of copper at $\omega = 0.5$.

the x-direction is increasing with the higher rate of increase and decrease near the outlet of the channel. Also, the values of the local Nusselt number are improved gradually by adding the volume fraction of the copper in the mixture. In both Figures 6(a) and 6(b), it can be understood that the increasing of the volume fraction of the aluminum oxide will always give favor to increasing the local Nusselt number along the x-direction.

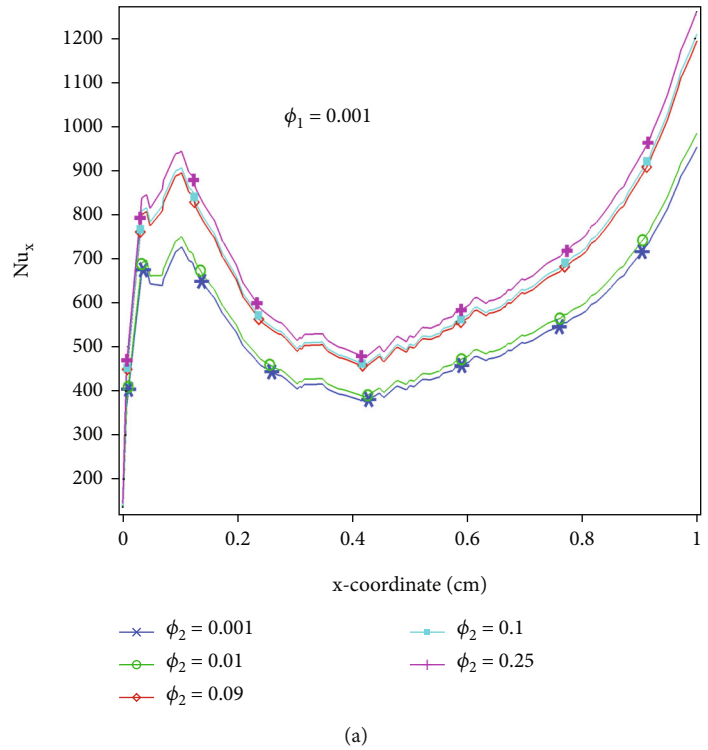

(a)

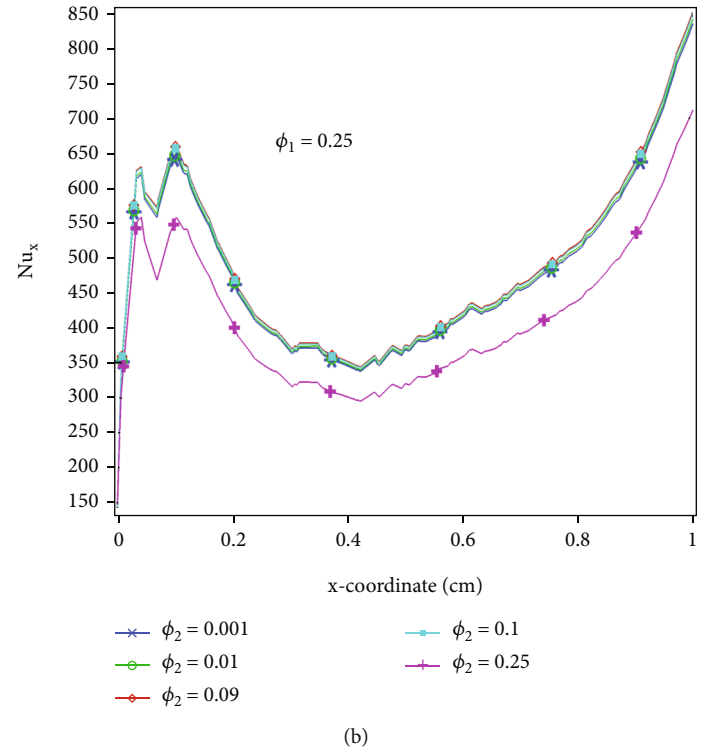

(b)

Figure 11: (a, b) Local Nusselt number along the length of the channel for all volume fractions of copper at $\omega = 1.5$.

Figures 7(a) and 7(b) are produced for $\omega = 0.5$ and $\phi_2 = 0.001, 0.25$. In the case in Figures 2(a) and 2(b), when we have obtained the simulation by increasing the rotational speed of perpendicular blocks, the local Nusselt number along the x-direction is increasing abruptly very near to the entrance of the channel and then decreases up to the middle of the channel and finally increases up to the exit of the channel. Unlike in the case discussed in Figures 6(a) and 6(b), in this case, the local Nusselt number is decreased with the increase in volume fraction

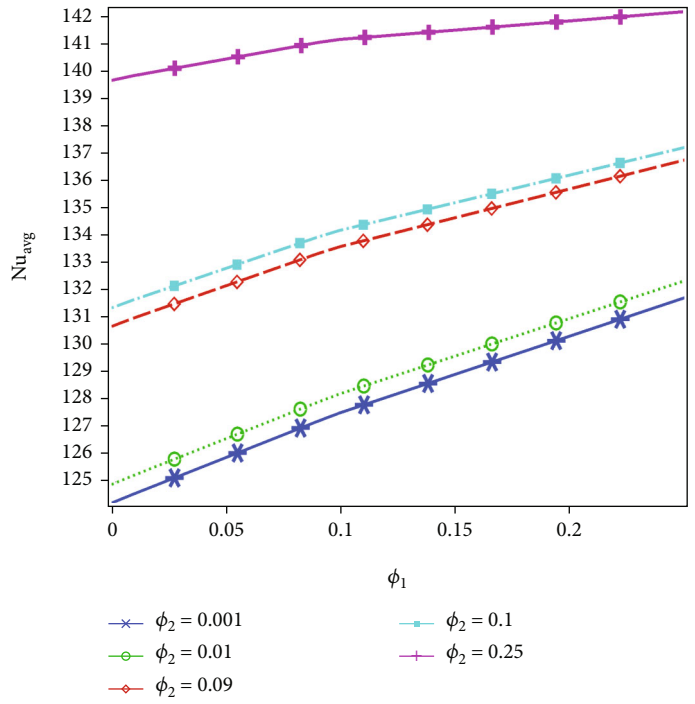

(a)

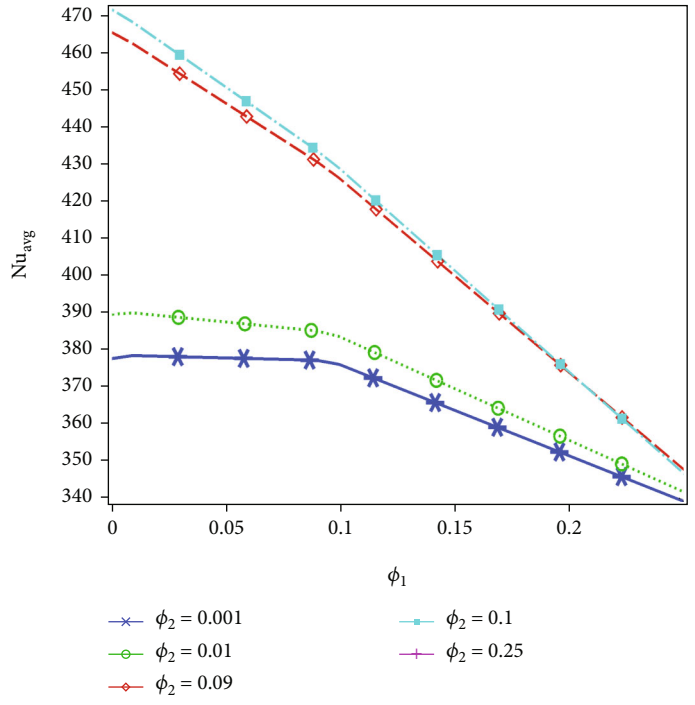

(b)

Figure 12: Continued.

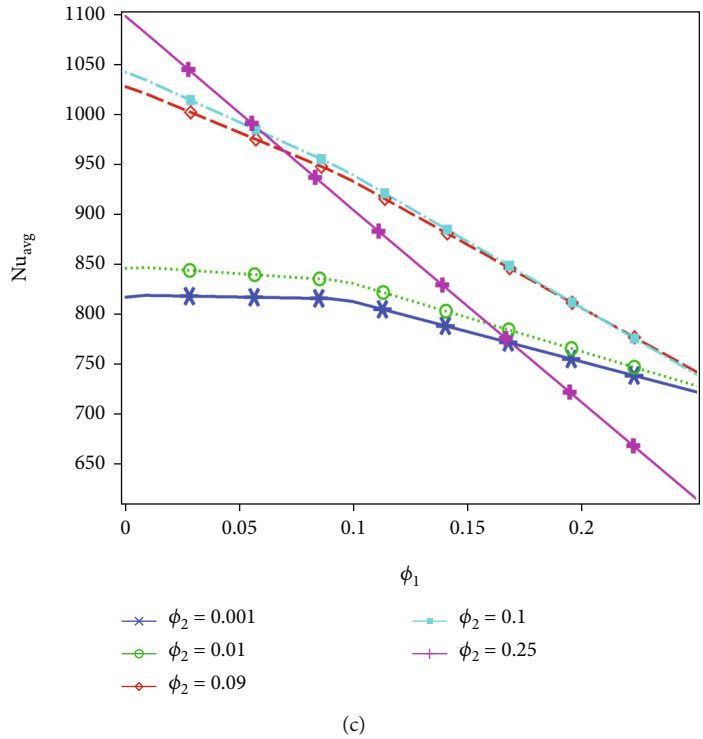

Figure 12: The average Nusselt number at the upper surface of the channel with the increasing volume fraction of the aluminum oxide: (a) $\omega = 0$, (b) $\omega = 0.5$, and (c) $\omega = 1.5$.

of aluminum oxide ϕ_1 from 0.001 to 0.25 as shown in both Figures 2(a) and 2(b). In Figure 7(b), it can be also seen that with increasing the volume fraction of copper, the pattern of the local Nusselt number is changed due to an increase in the volume fraction of alumina. Though, in this case, the local Nusselt number is decreasing with the increase in volume fraction, the pattern is obvious as compared in Figure 6(a). Moreover, the addition of the copper in the hybrid mixture by the fraction of 0.25 will increase the values of the local Nusselt number along the length of the channel.

In Figures 8(a) and 8(b), again we have focused on the pattern of the local Nusselt number with the increase in the rotation of perpendicular blocks by 1.5 in the domain and fixed the volume fraction of the copper by 0.001 and 0.25. The same pattern can be seen along the length of the channel; the local Nusselt number is increasing near the inlet in a very quick manner and then decreasing up to the middle of the channel and finally increasing up to the exit of the channel. But for the fixed volume fraction ϕ_2 of copper oxide, the local Nusselt number along the length of the channel is decreasing with an increase in the volume fraction of the aluminum oxide. Moreover, the speed of rotation of the perpendicular blocks will improve the local Nusselt number values along the length of the channel. It can be concluded that whenever the perpendicular blocks are not rotated, then the local Nusselt number at the exit of the channel is maximum; but when the block is rotating at the same speed, then the local Nusselt number at the outlet of the channel is maximum comparing Figures 6(a) and 6(b) and 7(a) and 7(b).

In Figures 9(a) and 9(b), the local Nusselt number is calculated by fixing the speed of rotation of the block and the volume fraction of the copper. It seems that with an increase in the volume fraction of the copper oxide in both cases of Figures 9(a) and 9(b) by fixing the volume fraction of the aluminum oxide, the local Nusselt number is always increasing along the channel and decreases up to the outlet of the channel. The addition of the aluminum oxide will boost the local Nusselt number along the length of the channel with the same pattern.

In Figures 10(a) and 10(b), the pattern of the local Nusselt number is checked by increasing the speed of rotation of the perpendicular blocks for a particular volume fraction of aluminum oxide. It is obvious that in Figure 10(a) the local Nusselt number is increasing abruptly near the inlet and is maximum at the outlet of the channel. The local Nusselt number is maximum at the outlet of the channel which means that the convection is maximum at the outlet of the channel. It can be seen that in Figure 10(a), with increasing the volume fraction of copper, the local Nusselt number is increasing. In Figure 10(b), it can be seen that adding more volume fraction of aluminum oxide will decrease the local Nusselt number by increasing the volume fraction of copper. Finally, we can see that the speed of rotation of the perpendicular blocks will increase the overall local Nusselt number along the length of the channel.

In Figures 11(a) and 11(b), the local Nusselt number along the length of the channel is presented by increasing

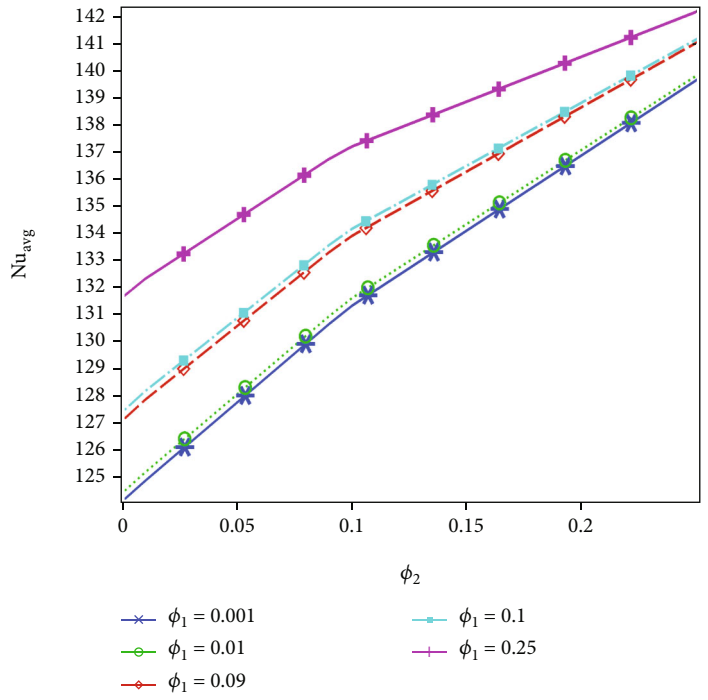

(a)

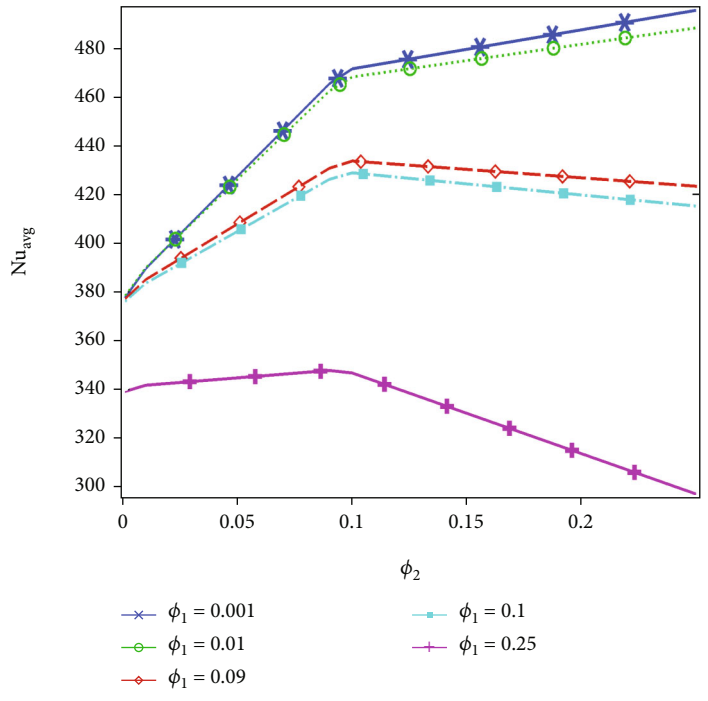

(b)

Figure 13: Continued.

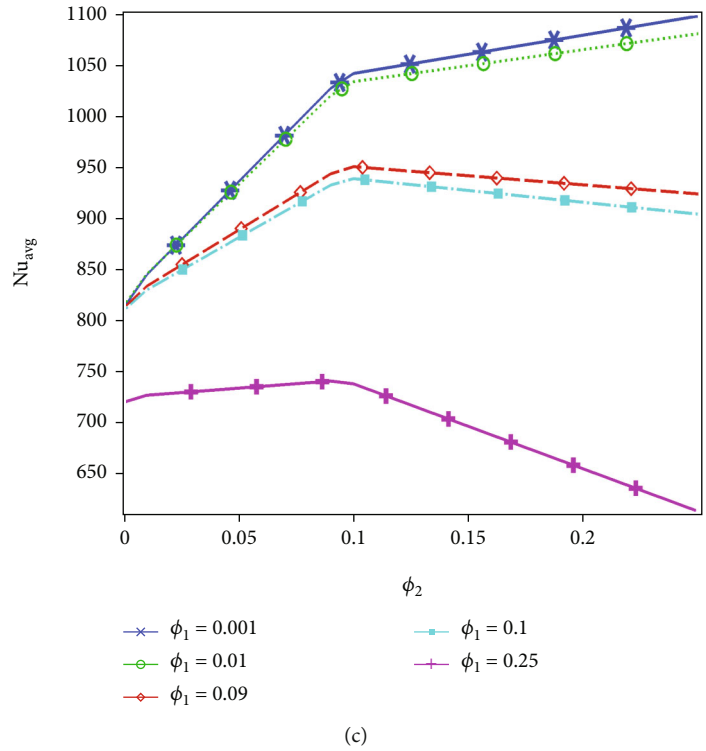

FIGURE 13: The average Nusselt number at the upper surface of the channel with the increasing volume fraction of the copper: (a) $\omega = 0$, (b) $\omega = 0.5$, and (c) $\omega = 1.5$.

the speed of rotation. It can be seen that with the increase in speed of rotation the local Nusselt number along the length of the channel is improved. Also, by adding the volume fraction of the aluminum oxide, the Nusselt number is decreasing by the values along the length of the channel. In Figure 11(a), when the volume fraction of alumina oxide was 0.001, the local Nusselt number is increasing at the outlet of the channel by increasing the volume fraction of the copper from 0.001 to 0.25. If we observe the local Nusselt number at the volume fraction of aluminum oxide at 0.25, the local Nusselt number is minimum at $\phi_2 = 0.25$.

The average Nusselt number against the volume fraction of alumina is calculated at the upper surface of the channel with a fixed volume fraction of the copper with 0.001-0.25 and with a variable speed of rotation of perpendicular blocks in Figures 12(a)–12(c). It can be seen that when $w = 0$ in Figure 12(a), the average Nusselt number is increasing at the upper surface of the channel. But, when the speed of the rotation of the perpendicular blocks is increased as in Figures 12(b) and 12(c), the average Nusselt number at the upper surface of the channel is decreasing. Therefore, it can be said that when the blocks are not moving, the convection is greater than conduction at the upper surface of the channel, and when they are in motion, the situation will be quite different.

In Figures 13(a)–13(c), the average Nusselt number at the upper surface of the rectangular channel has been determined by fixing the volume fraction of the aluminum oxide and rotation of the perpendicular blocks. These graphs perceived that with increasing the volume fraction of the copper, the average Nusselt number at the upper surface of the channel is increasing when the perpendicular blocks are stationary; see Figure 13(a). The pattern of the average Nusselt number is altered when the blocks are rotated $\omega = 0.5$ and 1.5; see Figures 13(b) and 13(c). It can be concluded that the average Nusselt number is increasing for the volume fraction of copper up to 0.1 and then decreasing. The process of declining becomes faster when the aluminum oxide is further added by the volume fraction ϕ_1. Therefore, in the cases when the blocks are rotating with some speed, with the addition of aluminum oxide in the copper, the average Nusselt number is decreasing with increasing the volume fraction of the copper.

5.2. Average Temperature and Gradient of Temperature along the z-Direction. Let μ be the total viscosity of the hybrid nanofluid that was calculated by fixing the volume fraction of the copper and the speed of rotation of the blocks. Now, we are determining the average temperature at the inlet of the channel in Figures 14(a)–14(d). From the graphs, it is obvious that the average temperature at the inlet of the channel is decreasing with the increasing viscosity of the hybrid nanofluid. Also, by increasing the speed of the perpendicular blocks, the average temperature along the middle of the channel further boosts up but shows the same behavior with increasing viscosity of hybrid nanofluids. Also, adding the copper by some volume fraction in the

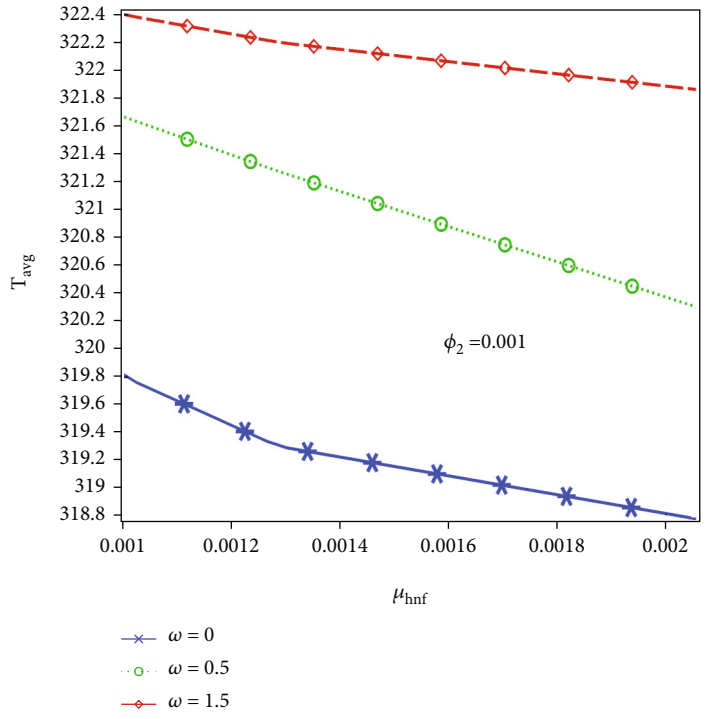

(a)

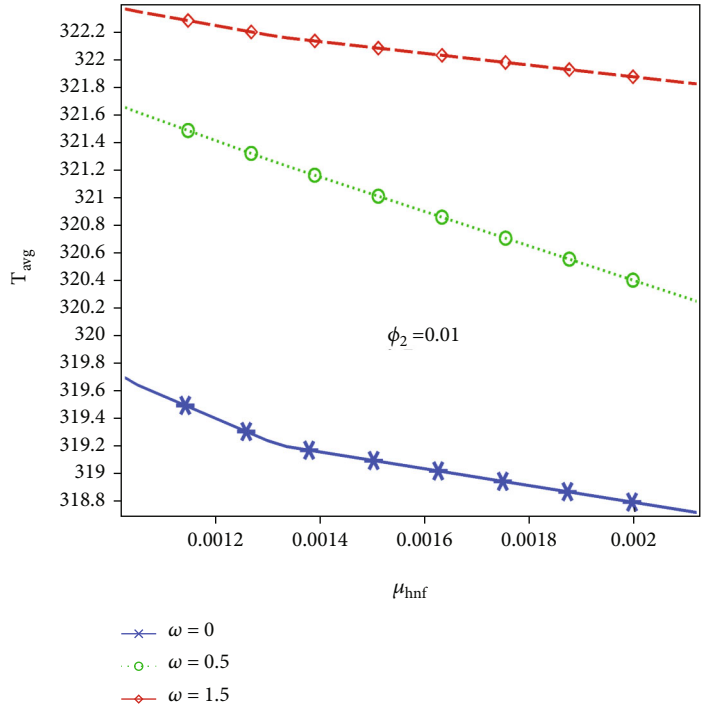

(b)

Figure 14: Continued.

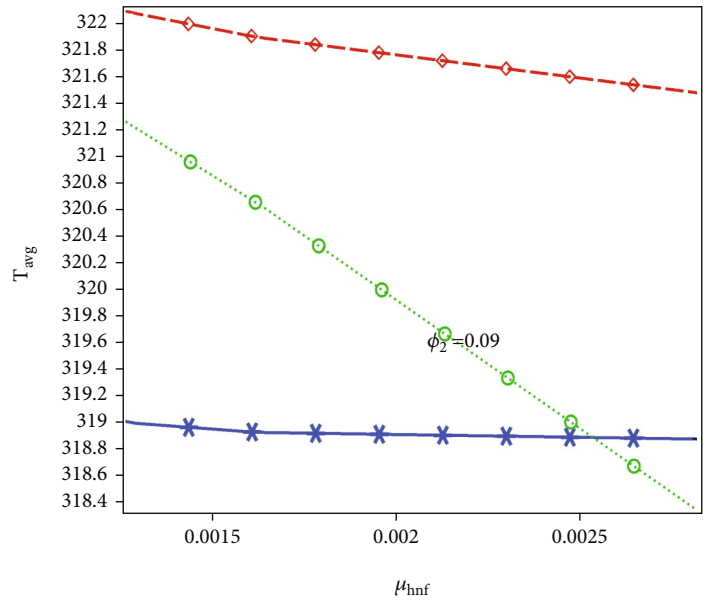

(c)

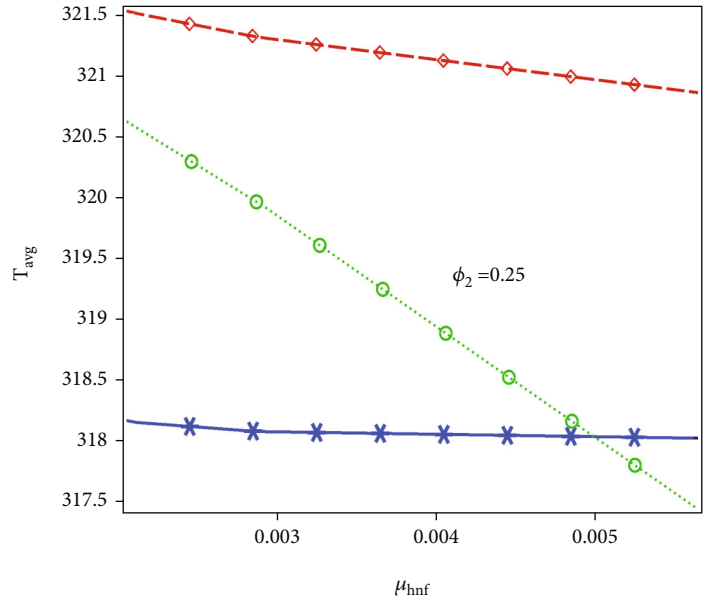

(d)

Figure 14: (a–d) Average temperature vs. the viscosity of the hybrid nanofluid at the inlet of the channel for all the volume fractions of aluminum oxide.

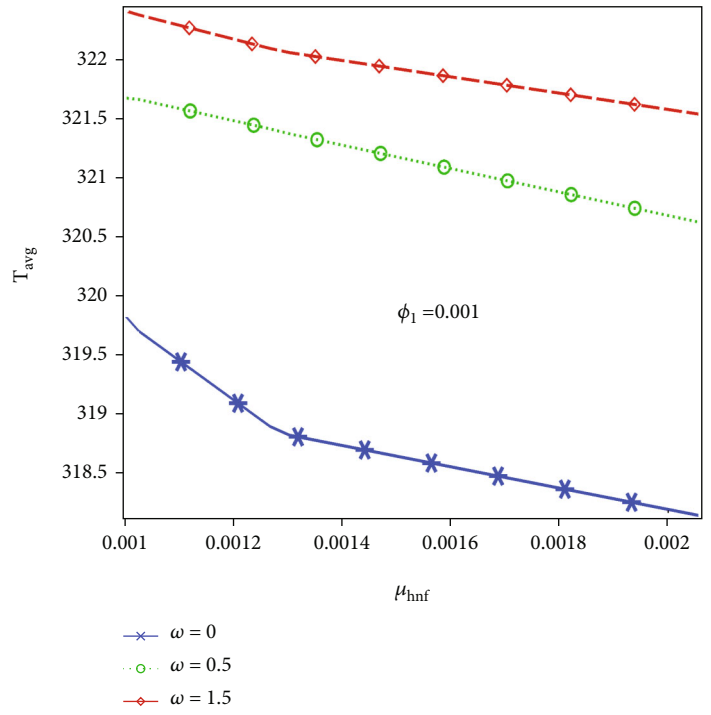

(a)

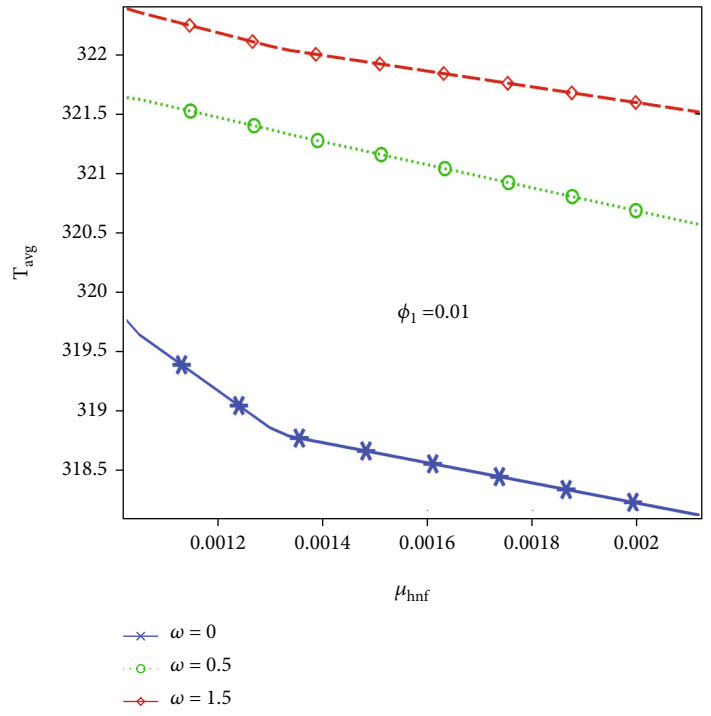

(b)

Figure 15: Continued.

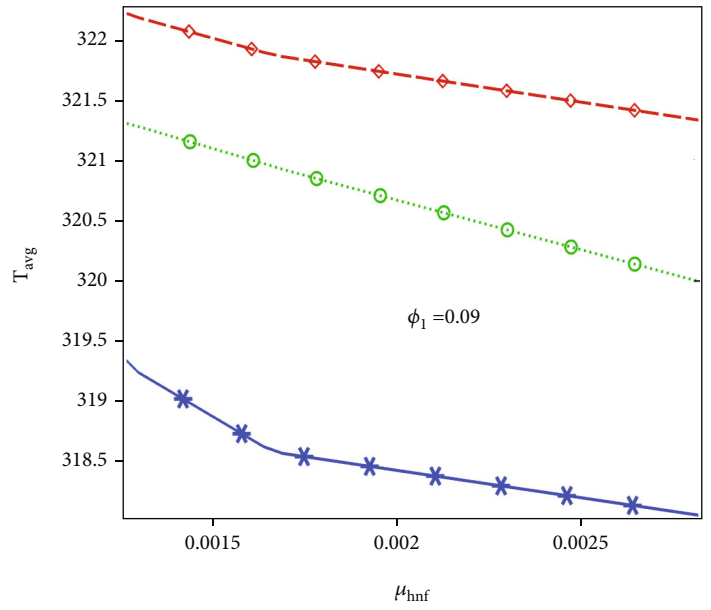

(c)

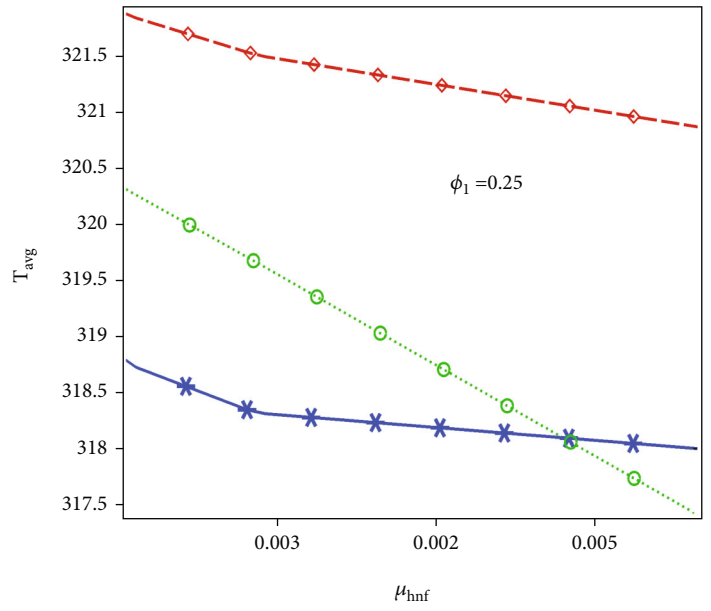

(d)

FIGURE 15: (a–d) Average temperature vs. the viscosity of the hybrid nanofluid at the inlet of the channel for all the volume fractions of copper.

Table 4: Average temperature at the inlet and the viscosity.

ϕ_1	ϕ_2	$\omega = 0$		$\omega = 0.5$		$\omega = 1.5$	
		μ (Pa·s)	T_{avg} (K)	μ (Pa·s)	T_{avg} (K)	μ (Pa·s)	T_{avg} (K)
0.001	**0.001**	**0.001003**	**319.82**	**0.001003**	**321.67**	**0.001003**	**322.4**
0.001	0.01	0.001026	319.7	0.001026	321.66	0.001026	322.37
0.001	0.09	0.001267	318.9	0.001267	321.41	0.001267	322.09
0.001	0.1	0.001302	318.82	0.001302	321.37	0.001302	322.05
0.001	0.25	0.002056	318.14	0.002056	320.62	0.002056	321.54
0.01	0.001	0.001026	319.76	0.001026	321.64	0.001026	322.39
0.01	0.01	0.00105	319.65	0.00105	321.62	0.00105	322.35
0.01	0.09	0.001299	318.86	0.001299	321.37	0.001299	322.07
0.01	0.1	0.001336	318.79	0.001336	321.33	0.001336	322.03
0.01	0.25	0.002119	318.13	0.002119	320.57	0.002119	321.52
0.09	0.001	0.001267	319.34	0.001267	321.31	0.001267	322.22
0.09	0.01	0.001299	319.24	0.001299	321.28	0.001299	322.18
0.09	0.09	0.001639	318.63	0.001639	320.97	0.001639	321.9
0.09	0.1	0.00169	318.57	0.00169	320.93	0.00169	321.86
0.09	0.25	0.00282	318.06	0.00282	320	0.00282	321.33
0.1	0.001	0.001302	319.29	0.001302	321.26	0.001302	322.2
0.1	0.01	0.001336	319.2	0.001336	321.23	0.001336	322.16
0.1	0.09	0.00169	318.6	0.00169	320.92	0.00169	321.87
0.1	0.1	0.001743	318.55	0.001743	320.87	0.001743	321.84
0.1	0.25	0.00293	318.05	0.00293	319.91	0.00293	321.31
0.25	0.001	0.002056	318.78	0.002056	320.31	0.002056	321.87
0.25	0.01	0.002119	318.72	0.002119	320.25	0.002119	321.83
0.25	0.09	0.00282	318.34	0.00282	319.7	0.00282	321.52
0.25	0.1	0.00293	318.31	0.00293	319.61	0.00293	321.48
0.25	*0.25*	*0.005646*	*318*	*0.005646*	*317.41*	*0.005646*	*320.86*

mixture will lead to a decline a little bit temperature at the inlet of the channel compared to Figures 14(a) and 14(d).

In Figures 15(a)–15(d), the average temperature is measured by fixing the volume fraction of the aluminum oxide and the speed of rotation of the perpendicular blocks, where μ present the viscosity of the hybrid nanofluid when the volume fraction of the copper in the mixture is varying from 0.001 to 0.25. As we found in Figure 15(a), the average temperature is quickly decreasing at the inlet of the channel with the increasing total viscosity of the channel when compared with Figure 14(a), although the addition of the aluminum fraction in the hybrid mixture will give additional support to the decline in the average temperature at the inlet of the channel. All cases can be compared in this regard. In Table 4, the maximum average temperature occurs when $\phi_1 = \phi_2 = 0.001$ (presented in bold) and the minimum average temperature occurs when $\phi_1 = \phi_2 = 0.25$ (presented in italic) for all the cases even if the blocks are rotating or stationary.

As in the current problem, a hybrid nanofluid along the rectangular channel contained the perpendicular moving blocks. A hot temperature was applied to the perpendicular blocks and a cool temperature condition was applied to the upper four-sided surfaces of the rectangular channel. In Figures 16(a)–16(d), the temperature gradient was expressed in terms of the volume fraction of aluminum oxide for a particular volume fraction of copper oxide and the rotational speed of the perpendicular blocks. It can be seen that when the perpendicular blocks are stationary, the temperature gradient along the z-direction is decreasing by increasing the volume fraction of aluminum oxide. As the rotational speed is increasing, the temperature gradient along the z-direction is increasing gradually with the increase of the volume fraction of aluminum oxide. Moreover, an addition of the copper in the mixture will support to decrease in the temperature gradient along the z-direction in the case when the perpendicular blocks are stationary. While the perpendicular blocks are rotating, the temperature gradient along the z-direction is increasing with the increase in volume fraction of the aluminum oxide. A great impact on the temperature gradient along the z-direction can be seen when the blocks are rotating at some speed ω which is obvious when comparing all the cases.

To examine the relationship of the temperature gradient along the z-direction with the volume fraction of copper, see Figures 17(a)–17(d). The temperature gradient along the z-direction is decreasing when the perpendicular blocks are stationary and increases when the perpendicular blocks

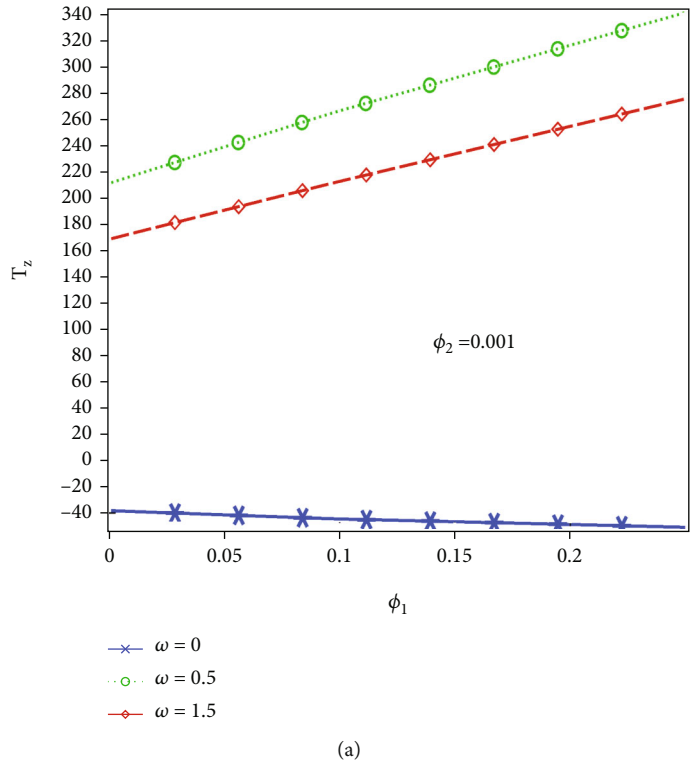

(a)

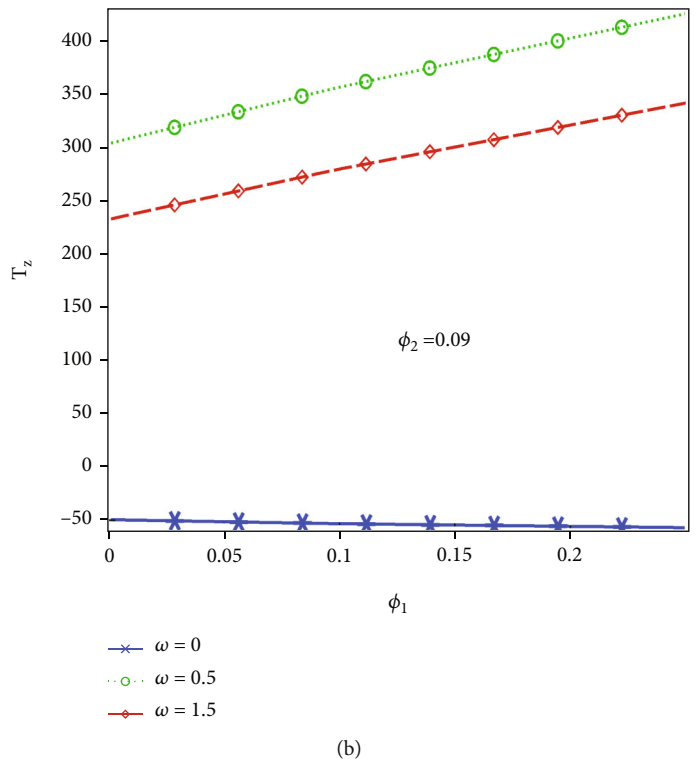

(b)

Figure 16: Continued.

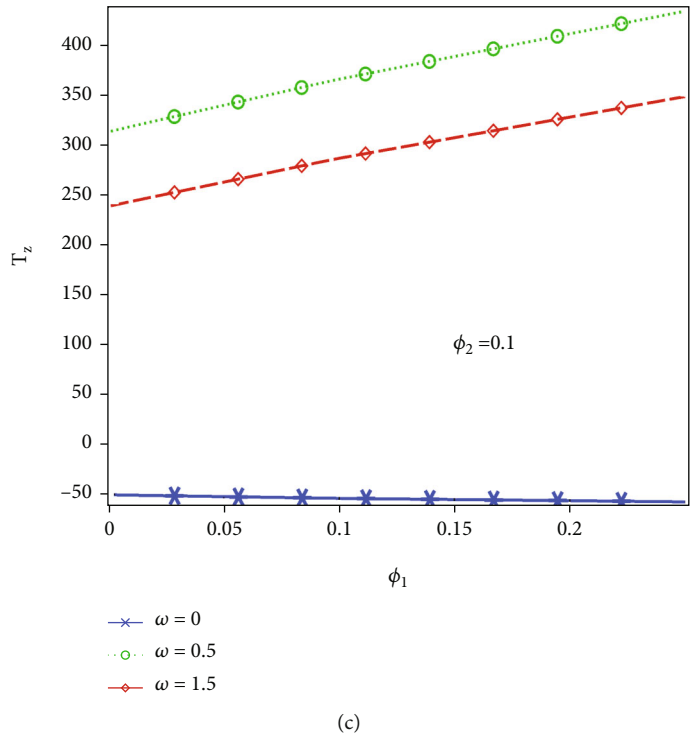

(c)

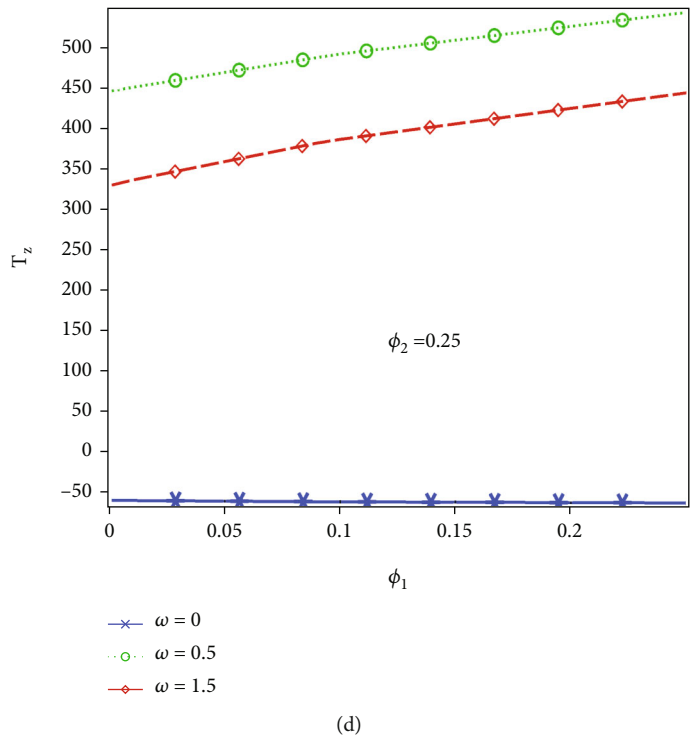

(d)

Figure 16: (a–d) Temperature gradient along the z-axis at the middle of the channel against the volume fraction of alumina oxide.

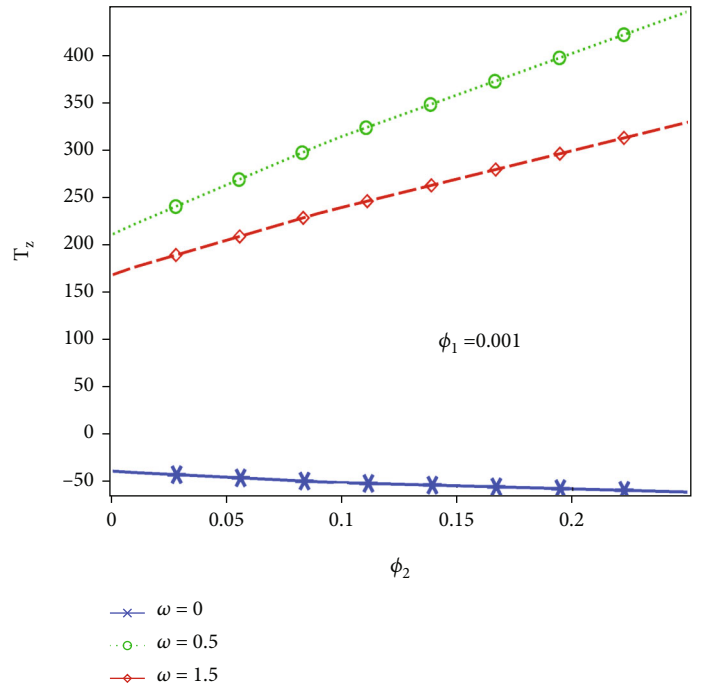

(a)

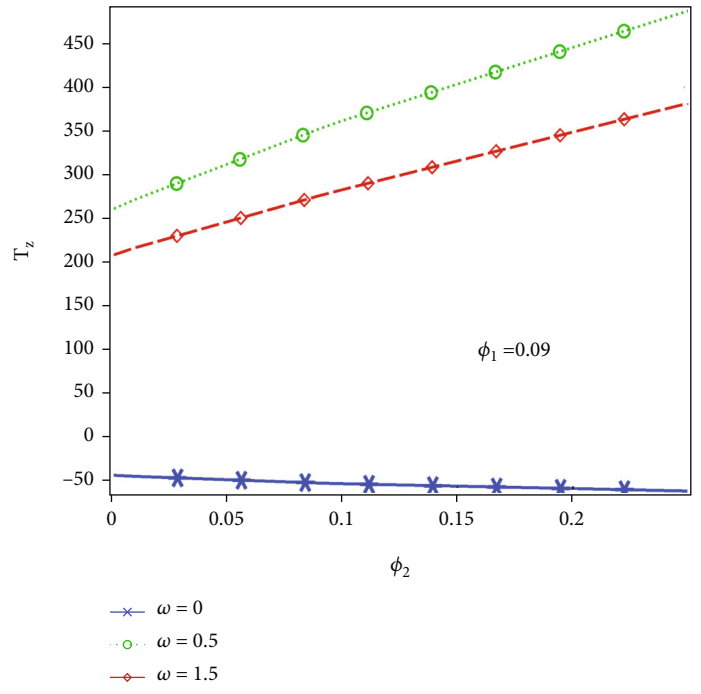

(b)

Figure 17: Continued.

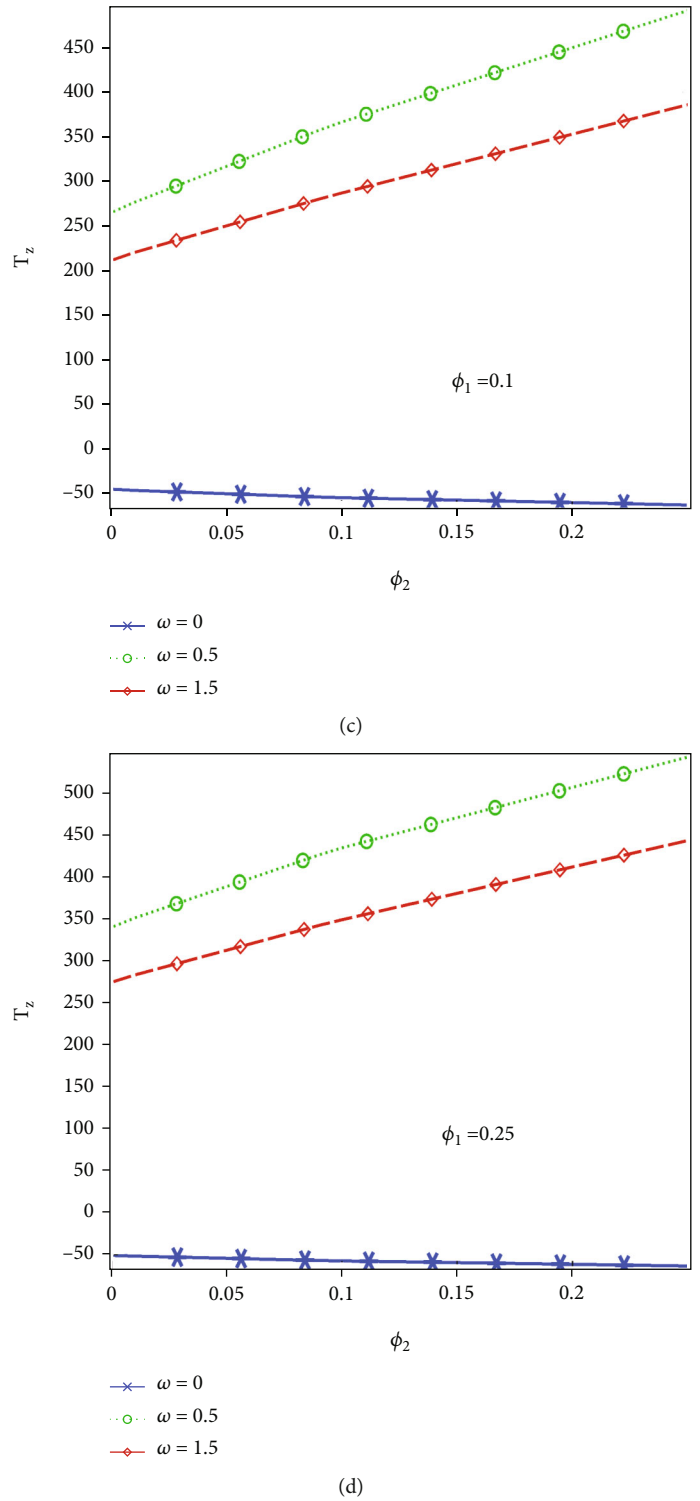

Figure 17: (a–d) Temperature gradient along the z-axis at the middle of the channel against the volume fraction of alumina oxide.

are moving with speed $\omega = 0.5$ and 1.5. The addition of the volume fraction of the alumina will lead to a decrease in the temperature gradient for the case when perpendicular blocks are stationary and an increase when the perpendicular blocks are rotating. From all this discussion, we can say that stationary perpendicular blocks are producing a cool environment inside the rectangular channel, while when they are moving, they are increasing the temperature gradient along the z-direction. The motion of the perpendicular blocks will take a great part in heat conduction over all the domains.

6. Conclusion

In the current article, we have analyzed the heat transfer in a three-dimensional rectangular channel containing the perpendicular rotating blocks when a hybrid nanofluid flows which contained a mixture of aluminum oxide and copper. Both the aluminum oxide and the copper were mixed in the volume fraction of 0.001-0.25 in the water base fluid. The study was done by the variation of the speed of rotation of the perpendicular rectangular blocks $\omega = 0$, 0.5, and 1.5. The governing partial differential equations of heat and the Navier-Stokes equations $\kappa - \varepsilon$ were used to develop the simulation into an emerging software COMSOL Multiphysics 5.6. The hybrid mixture was entered from the inlet of the channel with an average speed of Re = 50,000 whereas the turbulence dissipation rate ε and turbulence kinetic energy κ were kept in the range $3.46E-6$ to $3.76E-5$ and $2.50E-06$ to $1.23E-05$. The numerical results are validated by doing the mesh independent study and verified by comparing the average Nusselt number with the available correlations from the literature. The graphs and tables were used to present the numerical results for the local Nusselt number, average Nusselt number, average temperature, and average temperature gradient along the middle of the channel. We have reached the following decisions:

(i) For the fixed rotation of the perpendicular blocks and the volume fraction of copper, the local Nusselt number along the x-direction is increasing with the volume fraction of the aluminum oxide. For a stationary block, the local Nusselt number is found minimum at the outlet of the channel, and for rotational blocks, the local Nusselt number is maximum at the outlet of the channel

(ii) If blocks are rotating, then the volume fraction of the aluminum oxide will decrease the local Nusselt number along the x-direction. It was also perceived that when the blocks are rotating, the addition of the volume fraction of copper will increase the local number along the x-direction

(iii) The average Nusselt number at the upper surface of the channel is increasing by increasing the volume fraction of the aluminum oxide as well as the copper for stationary blocks and decreasing when the perpendicular blocks are in motion

(iv) The average temperature at the inlet of the channel is decreasing by increasing with the total viscosity of the hybrid nanofluid. The average temperature can be readily reduced by fixing the volume fraction of aluminum oxide and changing the volume fraction of copper

(v) Also, the average temperature at the inlet of the channel is increasing by increasing the speed of the rotation of the blocks. Moreover, the average temperature can be minimized by increasing the volume fraction of both nanoparticles

(vi) The temperature gradient along the z-direction is decreasing with the increase in volume fraction of both the nanofluids Al_2O_3 and Cu when the blocks are stationary. The rotational speed of the perpendicular blocks will be the cause to increase in the temperature gradient along the z-direction

Data Availability

No data were required to perform this research.

Conflicts of Interest

The authors declare that they have no conflict of interest.

Acknowledgments

This work was supported by Taif University Researchers Supporting Project Number (TURSP-2020/207), Taif University, Taif, Saudi Arabia.

References

[1] S. U. S. Choi, Z. G. Zhang, W. Yu, F. E. Lockwood, and E. A. Grulke, "Anomalous thermal conductivity enhancement in nanotube suspensions," *Applied Physics Letters*, vol. 79, no. 14, pp. 2252–2254, 2001.

[2] I. Khan, S. Fatima, M. Y. Malik, and T. Salahuddin, "Exponentially varying viscosity of magnetohydrodynamic mixed convection Eyring-Powell nanofluid flow over an inclined surface," *Results in Physics*, vol. 8, pp. 1194–1203, 2018.

[3] N. A. Halim, S. Sivasankaran, and N. F. M. Noor, "Active and passive controls of the Williamson stagnation nanofluid flow over a stretching/shrinking surface," *Neural Computing and Applications*, vol. 28, no. S1, pp. 1023–1033, 2017.

[4] A. K. Tiwari, S. Javed, H. F. Oztop, Z. Said, and N. S. Pandya, "Experimental and numerical investigation on the thermal performance of triple tube heat exchanger equipped with different inserts with WO_3/water nanofluid under turbulent condition," *International Journal of Thermal Sciences*, vol. 164, article 106861, 2021.

[5] N. S. Pandya, H. Shah, M. Molana, and A. K. Tiwari, "Heat transfer enhancement with nanofluids in plate heat exchangers: a comprehensive review," *European Journal of Mechanics-B/Fluids*, vol. 81, pp. 173–190, 2020.

[6] Z. Said, S. Sundar, A. K. Tiwari et al., *Recent advances on the fundamental physical phenomena behind stability, dynamic motion, thermophysical properties, heat transport, applications, and challenges of nanofluids*, Physics Reports, 2021.

[7] S. Samiezadeh, R. Khodaverdian, M. H. Doranehgard, H. Chehrmonavari, and Q. Xiong, "CFD simulation of thermal performance of hybrid oil-Cu-Al2O3 nanofluid flowing through the porous receiver tube inside a finned parabolic trough solar collector," *Sustainable Energy Technologies and Assessments*, vol. 50, article 101888, 2022.

[8] Z. Said, N. K. Cakmak, L. Prabhakar Sharma, and S. Sundar, "Synthesis, stability, density, viscosity of ethylene glycol-based ternary hybrid nanofluids: experimental investigations and model -prediction using modern machine learning techniques," *Powder Technology*, vol. 400, article 117190, 2022.

[9] S. Suresh, K. P. Venkitaraj, P. Selvakumar, and M. Chandrasekar, "Effect of Al_2O_3-Cu/water hybrid nanofluid in heat transfer," *Experimental Thermal and Fluid Science*, vol. 38, pp. 54–60, 2012.

[10] M. Baghbanzadeh, A. Rashidi, D. Rashtchian, R. Lotfi, and A. Amrollahi, "Synthesis of spherical silica/multiwall carbon nanotubes hybrid nanostructures and investigation of thermal conductivity of related nanofluids," *Thermochimica Acta*, vol. 549, pp. 87–94, 2012.

[11] D. Wen and Y. Ding, "Experimental investigation into convective heat transfer of nanofluids at the entrance region under laminar flow conditions," *International Journal of Heat and Mass Transfer*, vol. 47, no. 24, pp. 5181–5188, 2004.

[12] X.-Q. Wang and A. S. Mujumdar, "Heat transfer characteristics of nanofluids: a review," *International Journal of Thermal Sciences*, vol. 46, no. 1, pp. 1–19, 2007.

[13] S. Heris and S. Zeinali, "Experimental investigation of oxide nanofluids laminar flow convective heat transfer," *International communications in heat and mass transfer*, vol. 33, no. 4, pp. 529–535, 2006.

[14] S. Z. Heris, S. G. Etemad, and M. N. Esfahany, "Experimental investigation of convective heat transfer of Al2O3/water nanofluid in circular tube," *International journal of heat and fluid flow*, vol. 28, no. 2, pp. 203–210, 2007.

[15] F. Mabood and A. T. Akinshilo, "Stability analysis and heat transfer of hybrid Cu- Al_2O_3/H_2O nanofluids transport over a stretching surface," *International Communications in Heat and Mass Transfer*, vol. 123, article 105215, 2021.

[16] S. Lee, S. U. S. Choi, S. Li, and J. A. Eastman, "Measuring thermal conductivity of fluids containing oxide nanoparticles," pp. 280–289, 1999.

[17] V. Sridhara and L. N. Satapathy, "Al_2O_3-based nanofluids: a review," *Nanoscale Research Letters*, vol. 6, no. 1, pp. 1–16, 2011.

[18] Z. Said, M. H. Sajid, M. A. Alim, R. Saidur, and N. A. Rahim, "Experimental investigation of the thermophysical properties of AL_2O_3-nanofluid and its effect on a flat plate solar collector," *International Communications in Heat and Mass Transfer*, vol. 48, pp. 99–107, 2013.

[19] M. N. Rostami, S. Dinarvand, and I. Pop, "Dual solutions for mixed convective stagnation-point flow of an aqueous silica-alumina hybrid nanofluid," *Chinese Journal of Physics*, vol. 56, no. 5, pp. 2465–2478, 2018.

[20] R. Taherialekouhi, S. Rasouli, and A. Khosravi, "An experimental study on stability and thermal conductivity of water-graphene oxide/aluminum oxide nanoparticles as a cooling hybrid nanofluid," *International Journal of Heat and Mass Transfer*, vol. 145, article 118751, 2019.

[21] P. K. Jena, E. A. Brocchi, and M. S. Motta, "In-situ formation of Cu-Al_2O_3 nano-scale composites by chemical routes and studies on their microstructures," *Materials Science and Engineering: A*, vol. 313, no. 1-2, pp. 180–186, 2001.

[22] K. Niihara, "New design concept of structural ceramics," *Journal of the Ceramic Society of Japan*, vol. 99, no. 1154, pp. 974–982, 1991.

[23] S. Suresh, K. P. Venkitaraj, and P. Selvakumar, "Synthesis, characterisation of Al_2O_3-Cu nano composite powder and water based nanofluids," *Advanced Materials Research*, vol. 328-330, pp. 1560–1567, 2011.

[24] S.-T. Oh, T. Sekino, and K. Niihara, "Fabrication and mechanical properties of 5 vol% copper dispersed alumina nanocomposite," *Journal of the European Ceramic Society*, vol. 18, no. 1, pp. 31–37, 1998.

[25] P. Selvakumar and S. Suresh, "Use of ${\rm Al}_{2}{\rm O}_{3}\hbox{–}{\rm Cu}$/water hybrid nanofluid in an electronic heat sink," *IEEE Transactions on Components, Packaging and Manufacturing Technology*, vol. 2, no. 10, pp. 1600–1607, 2012.

[26] A. Ijam, R. Saidur, and P. Ganesan, "Cooling of minichannel heat sink using nanofluids," *International Communications in Heat and Mass Transfer*, vol. 39, no. 8, pp. 1188–1194, 2012.

[27] C.-J. Ho and W. C. Chen, "An experimental study on thermal performance of Al_2O_3/water nanofluid in a minichannel heat sink," *Applied Thermal Engineering*, vol. 50, no. 1, pp. 516–522, 2013.

[28] M. S. Tahat and A. C. Benim, "Experimental analysis on thermophysical properties of Al_2O_3/CuO hybrid nano fluid with its effects on flat plate solar collector," in *In Defect and diffusion forum*, vol. 374, pp. 148–156, Trans Tech Publications Ltd, 2017.

[29] A. Yegane, S. Pooya, and A. Kasaeian, "Thermal performance assessment of a flat-plate solar collector considering porous media, hybrid nanofluid and magnetic field effects," *Journal of Thermal Analysis and Calorimetry*, vol. 141, no. 5, pp. 1969–1980, 2020.

[30] A. Azman, M. Z. Yusoff, A. Mukhtar, P. Gunnasegaran, N. A. Hamid, and N. K. Ching, "Numerical study of heat transfer enhancement for mono and hybrid nanofluids flow in a straight pipe," *CFD Letters*, vol. 13, no. 2, pp. 49–61, 2021.

[31] F. W. Dittus and L. M. K. Boelter, "Heat transfer in automobile radiators of the tubular type," *International Communications in Heat and Mass Transfer*, vol. 12, no. 1, pp. 3–22, 1985.

[32] A. Bejan, *Convection heat transfer*, John Wiley & sons, 2013.

[33] E. N. Sieder and G. E. Tate, "Heat transfer and pressure drop of liquids in tubes," *Industrial & Engineering Chemistry*, vol. 28, no. 12, pp. 1429–1435, 1936.

[34] Q. Li and Y. Xuan, "Convective heat transfer and flow characteristics of Cu-water nanofluid," *Science in China Series E: Technological Science*, vol. 45, no. 4, pp. 408–416, 2002.

[35] D. Taler and J. Taler, "Simple heat transfer correlations for turbulent tube flow," in *E3S Web of conferences*, vol. 13, p. 02008, EDP Sciences, 2017.